SISSA

PAPER • OPEN ACCESS

Measurements of sensor radiation damage in the ATLAS inner detector using leakage currents

To cite this article: The ATLAS collaboration *et al* 2021 *JINST* **16** P08025

View the article online for updates and enhancements.

Measurements of sensor radiation damage in the ATLAS inner detector using leakage currents

The ATLAS collaboration

E-mail: atlas.publications@cern.ch

ABSTRACT: Non-ionizing energy loss causes bulk damage to the silicon sensors of the ATLAS pixel and strip detectors. This damage has important implications for data-taking operations, charged-particle track reconstruction, detector simulations, and physics analysis. This paper presents simulations and measurements of the leakage current in the ATLAS pixel detector and semiconductor tracker as a function of location in the detector and time, using data collected in Run 1 (2010–2012) and Run 2 (2015–2018) of the Large Hadron Collider. The extracted fluence shows a much stronger $|z|$-dependence in the innermost layers than is seen in simulation. Furthermore, the overall fluence on the second innermost layer is significantly higher than in simulation, with better agreement in layers at higher radii. These measurements are important for validating the simulation models and can be used in part to justify safety factors for future detector designs and interventions.

Contents

1 Introduction

The ATLAS pixel and strip detectors are the subdetectors in closest proximity to the interaction point and are exposed to an unprecedented amount of radiation. Monitoring and modelling the bulk radiation damage in the pixel and strip detector sensors is crucial for many aspects of the ATLAS experiment [1] including radiation protection, determination of operational conditions, offline data

analysis, and upgrade design. Understanding the impact of radiation damage will help extend the lifetime and optimal use of the detectors. Sensors designed for the high-luminosity phase of the Large Hadron Collider (LHC) will need to cope with about an order of magnitude more fluence than the present detector and thus investigations with the current detector will provide valuable input to preparations for those data-taking conditions in the near future.

One of the best-characterized methods for monitoring silicon radiation damage is based on measuring the sensor leakage current. This paper documents measurements of the sensor leakage current in the ATLAS pixel and strip detectors for the entire first and second runs of the LHC. Models of thermal annealing combined with temperature and luminosity histories in data are used to extract the measured fluence across detector regions. These data are compared with simulations of radiation damage that model particle production, propagation through the sensors, and bulk damage. Thermal annealing models can be used to extract the fluence from data for comparison with simulations or annealing models and can be combined with simulations to compare with measured leakage currents directly. Complementary studies related to the detailed modelling of the sensor response to deposited charge from minimum-ionizing particles can be found in ref. [2].

This paper is organized as follows. Section 2 introduces the ATLAS pixel and strip detectors and reviews the effects of radiation damage on their sensors. Next, section 3 describes how the complex radiation fields inside the ATLAS inner detector can be modelled and how the corresponding damage leads to changes in the sensor leakage current. Technical details of the measurements for each subdetector are presented in section 4. All of the measurements are compared in section 5. The paper ends with the conclusions and outlook in section 6.

2 The ATLAS inner-detector silicon sensors and radiation damage effects

The ATLAS inner detector is composed of three subdetectors immersed in a 2 T magnetic field for measuring the trajectories of charged particles. The two innermost subdetectors are based on silicon pixel and strip sensors, respectively. Figure 1 illustrates the radial extent of the pixel detector, the strip detector (called the semiconductor tracker or SCT) and transition radiation tracker (TRT).

The ATLAS pixel detector [1, 3–5] consists of four barrel layers and two identical endcap regions, each with three disk layers. The layers are composed primarily of n^+-in-n planar oxy-genated [6, 7] silicon sensors. The four barrel layers, labelled Insertable B-Layer (IBL) [4, 5], B-Layer, Layer-1 and Layer-2, are arranged in concentric cylinders at radii of 33.25, 50.5, 88.5, and 122.5 mm from the beam axis. While most of the pixel detector was installed before the start of LHC Run 1, the innermost barrel layer, IBL, was installed during the shutdown (LS1) between LHC Run 1 and Run 2. Most of the sensors in the pixel detector (IBL) are 250 (200) μm thick with a traditional planar geometry. At high |z| values[1] the IBL contains n^+-in-p 3D sensors [8] that are 230 μm thick. The pixel pitch is 50×250 μm^2 for the IBL and 50×400 μm^2 for the other pixel layers.

---

[1]ATLAS uses a right-handed coordinate system with its origin at the nominal interaction point (IP) in the centre of the detector and the z-axis coinciding with the axis of the beam pipe. The x-axis points from the IP towards the centre of the LHC ring, and the y-axis points upward. Cylindrical coordinates (r, ϕ) are used in the transverse plane, ϕ being the azimuthal angle around the z-axis. The pseudorapidity is defined in terms of the polar angle θ as $\eta = -\ln\tan(\theta/2)$.
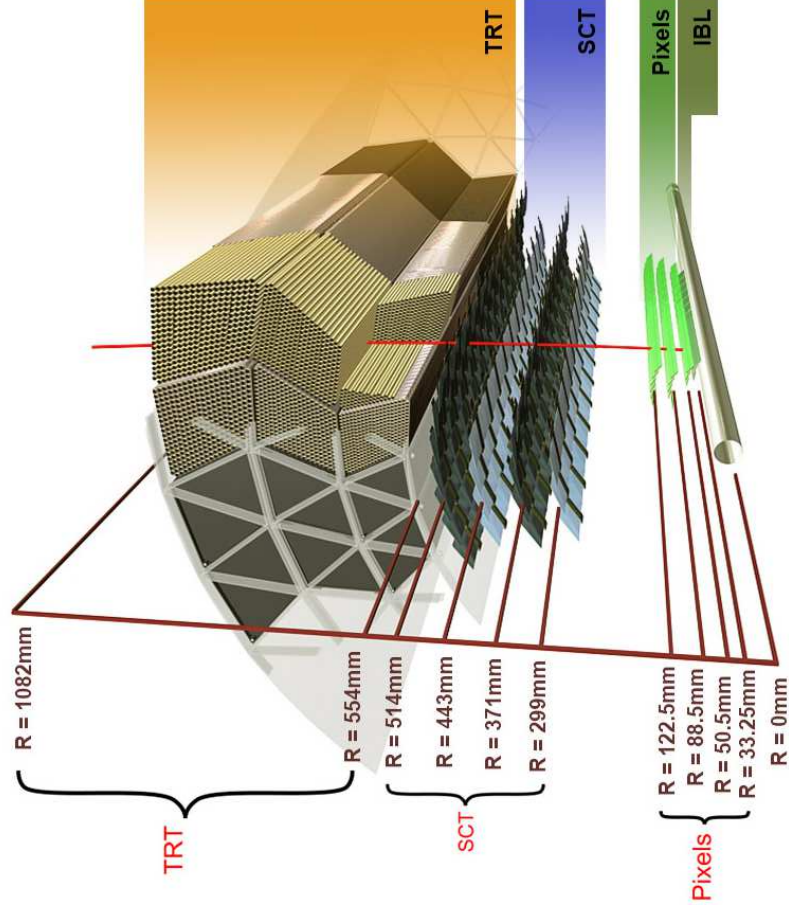
Figure 1. A schematic view of the ATLAS inner detector. Radially outward from the collision point are the ATLAS insertable B-layer (IBL), the other layers of the pixel detector, the semiconductor microstrip tracker SCT, and the transition radiation tracker (TRT). A red curved line represents a charged particle traversing the various layers and bending in the 2 T magnetic field. The innermost pixel layer is called the Insertable B-Layer and was added to the detector between the first and second runs of the LHC.

The SCT [1, 9–12] consists of four barrel layers and two endcaps, with nine disks each. The four barrel layers are located at 29.9, 37.1, 44.3, and 51.4 cm from the centre of the ATLAS detector and the disks are located at $|z|$ values ranging from 74.9 cm to 272 cm in order to provide tracking coverage up to $|\eta| = 2.5$. All of the modules are composed of pairs of sensors offset by 40 mrad; this stereo angle provides space-point information. The sensors have a pitch of 80 μm and are 285 μm thick. Each sensor is constructed of high-resistivity n-type bulk silicon with p-type implants.

Radiation damage in the sensor bulk is primarily caused by displacement of a silicon atom from of its lattice site, resulting in a silicon interstitial site and a leftover vacancy (Frenkel pair) [13, 14]. These primary defects build, depending on the recoil energy, cluster defects and point defects in the silicon lattice that produce energy levels in the band gap. When activated and occupied, these states increase the sensor leakage current (I_{leak}), which is proportional to the fluence received: $\Delta I_{\text{leak}} = \alpha \, \Phi_{\text{eq}} \, V$, where the effective fluence, Φ_{eq}, is the 1 MeV neutron equivalent fluence defined as the number of 1 MeV neutrons applied to a sensor of surface area 1 cm^2 that cause damage equivalent to that from all particles that traversed the sensor. The volume V is the depleted volume of the silicon sensor and α is the current-related damage coefficient. The goal of this measurement is to compare I_{leak} with predictions of Φ_{eq}, either by transforming the leakage current to a fluence or by transforming the fluence into a leakage current via α.

– 3 –

3 Simulations

3.1 Radiation simulations

The complex radiation fields inside the ATLAS inner detector are simulated by propagating particles from inelastic proton-proton interactions, generated by PYTHIA 8 [15, 16] using the MSTW2008LO parton distribution functions [17] and the A3 set of tuned parameters [18], through the ATLAS detector material using the particle transport code FLUKA [19, 20] or GEANT4 [21]. The particle and energy spectra are then folded with silicon damage factors from the RD50 database [22–26] to compute the 1 MeV neutron equivalent damage. The tabulated weights cover neutrons, protons, charged pions and electrons. For charged kaons the pion weights are used, while for anti-neutrons, anti-protons, baryons and ions the proton weights are used and positrons are treated like electrons.

The FLUKA and GEANT4 programs are composed of many subroutines based on a variety of phenomenological and first-principles models for nuclear and electromagnetic interactions of particles with the ATLAS detector material. The most important difference from the point of view of particle propagation is the detector geometry, which slightly differs between the two programs as is explained in more detail below.

3.1.1 FLUKA

The FLUKA code [27, 28] is well-established for studies of hadronic and electromagnetic cascades induced by high-energy particles and is the baseline code for radiation background simulations at CERN and the LHC experiments. Electrons, photons and muons up to 1000 TeV, and hadrons up to 20 TeV, can undergo interactions and be transported. The lower cut-offs in energy for particle transport in the FLUKA simulations are: hadrons and muons 100 keV; neutrons 10^{-5} eV (thermal); photons 30 keV; and electrons 100 keV. However, photons and electrons have higher cut-offs in some regions (collimators, forward shielding) to reduce simulation time. Anti-particles, heavy ions and residual nuclei production are also treated by FLUKA.

A complete description of FLUKA's physics models and capabilities can be found in ref. [29] and references therein. For example, inelastic hadron interactions are described by different physics models depending on the energy. Inelastic hadron-hadron interactions above 5 GeV are treated by the Dual Parton Model [30], and below 5 GeV by the resonance production and decay model [31]. For hadron-nucleus inelastic interactions above 5 GeV, Glauber-Gribov multiple scattering followed by Generalized Intranuclear Cascade is employed. Below 5 GeV the pre-equilibrium cascade model PEANUT is used [32, 33]. All the above hadron interaction models include evaporation and gamma de-excitation of the residual nucleus [34, 35]. Light residual nuclei are not evaporated, but are fragmented into a maximum of six bodies according to a Fermi break-up model.

A description of the full ATLAS detector geometry and material has evolved in FLUKA over the past 20 years, and includes shielding, beam-line and machine components. This has been developed independently of the ATLAS GEANT4 geometry described below, and in some cases has been simplified to speed up the simulations, e.g. by using cylinders to describe detector barrel layers. In parts a three-dimensional geometry with ϕ-asymmetry is implemented when considered important for providing more accurate predictions. The magnetic fields are imported from the ATLAS offline software.

3.1.2 GEANT4

GEANT4 [21] is used as the standard simulation toolkit for physics analysis in ATLAS. The implementation of the detector geometry is therefore very detailed, especially for instrumented regions and regions relevant for the signal response, including upstream non-instrumented areas. The advent of new 'physics lists' in GEANT4 with high-precision transport of neutrons and the possibility to simulate activation of nuclides and their radioactive decay from timescales of nanoseconds to billions of years makes GEANT4 an attractive option for simulating the radiation background.

Various physics lists are used to determine the models and precision for processes simulated by GEANT4. Hadronic physics is governed by the FTFP_BERT list, which includes the Fritiof model [36–39] with a precompound model above 4 GeV and the Bertini intra-nuclear cascade model below 5 GeV. Energy thresholds are implemented via range cuts, whereby if the expected range of a secondary is less than some minimum value, the energy of that secondary particle is deposited at the end of the primary particle's step and no separate secondary is produced. The range cuts vary from tens of microns to 1 mm depending on the subdetector material.

The geometry description for the ATLAS GEANT4 simulation uses GEOMODEL [40], a library of basic geometrical shapes, to describe and construct the detector. This model is the same one used for data analysis in ATLAS and is highly detailed for all detector components, including both active and passive material. For the actual simulation, the geometry is translated entirely from the GEOMODEL to the GEANT4 format. Further details about the ATLAS GEANT4 simulation can be found in ref. [41].

3.2 Modelling leakage current and annealing

The formula $\Delta I_{\text{leak}} = \alpha\, V\, \Phi_{\text{eq}}$ only applies to instantaneous irradiation, where α is approximately independent of the damaging particles' energies and flavours. After some time t at a temperature T, the leakage current changes because of defect annealing, so $\alpha = \alpha(t, T)$. Different models vary in their treatment of α. The model used to compare with all silicon layers is the Hamburg Model [13], as implemented in ref. [42], where for n time intervals, the predicated leakage current is given by

$$I_{\text{leak}} = (\Phi/L_{\text{int}}) \cdot \sum_{i=1}^{n} V_i \cdot L_{\text{int},i} \cdot \left[\alpha_I \exp\left(-\sum_{j=i}^{n} \frac{t_j}{\tau(T_j)}\right) + \alpha_0^* - \beta \log\left(\sum_{j=i}^{n} \frac{\Theta(T_j) \cdot t_j}{t_0}\right) \right], \qquad (3.1)$$

where $L_{\text{int},i}$ is the integrated luminosity, t_i is the duration, and T_i is the temperature in time interval i. The first sum is over all time periods and the two sums inside the exponential and logarithm functions are over the time between the irradiation in time period i and the present time. The other symbols in eq. (3.1) are $t_0 = 1$ min, $V_i =$ depleted volume (in cm^3), $\alpha_I = (1.23\pm0.06)\times10^{-17}$ A/cm, τ follows an Arrhenius equation $\tau^{-1} = (1.2^{+5.3}_{-1.0}) \times 10^{13}$ s$^{-1} \times e^{(-1.11\pm0.05)\,eV/k_B T}$, where k_B is the Boltzmann constant, $\alpha_0^* = 7.07 \times 10^{-17}$ A/cm, and $\beta = (3.29 \pm 0.18) \times 10^{-18}$ A/cm.[2] Note that the α and β parameters are degenerate with the silicon damage factors, which are not well-known (see

---

[2] A small temperature dependence has been observed in the value of β [13]. For this analysis, the reported value at 21 °C is used as it is closest to the operational temperature range of the detector.

section 5.1). The temperature scaling function $\Theta(T)$ is defined by[3]

$$\Theta(T) = \exp\left[-\frac{E_I^*}{k_B}\left(\frac{1}{T} - \frac{1}{T_{\text{ref}}}\right)\right],\tag{3.2}$$

where $E_I^* = (1.30 \pm 0.14)$ eV and T_{ref} is a reference temperature.

The value of the fluence rate, Φ/L_{int}, in data is estimated by performing a fit using eq. (3.1) and letting only this parameter float. The value Φ/L_{int} can be predicted from the PYTHIA+FLUKA or GEANT4 simulations. When this value is used, the resulting predictions are called 'unscaled'. It is useful to fit a scale factor to this value instead of fitting Φ/L_{int} without any prior. The simulation normalized with a scale factor obtained from a fit to data are defined as "scaled" in the following.

4 Measurements

4.1 General inputs and corrections

4.1.1 Luminosity

Luminosity data are collected approximately once per minute. The luminosity scale is determined by a set of dedicated bunch-by-bunch luminosity detectors [44] that are calibrated using the van der Meer method [45]. The absolute luminosity used in this study accounts for luminosities accumulated during times when the ATLAS detector is operating and also when it is not operating, because all particle fluence received by the silicon sensors will impact the leakage current. Luminosities used for this study surpass the quantities reported as the official ATLAS integrated luminosity usable for physics.

The uncertainty in the luminosity does not contribute to uncertainty in the leakage current data but is included in the fluence measurement. The uncertainty in the combined 2015–2018 integrated luminosity is 1.7% [46], obtained using the LUCID-2 detector [47] for the primary luminosity measurements.

A series of quality criteria are applied to the leakage current data considered in subsequent sections. Leakage current data are excluded for modules during periods when their bias voltage was not applied. Data collected within one minute of high-voltage turn-on are also excluded. Analysis of the leakage current data is restricted to times when the LHC has declared the proton beams to be stable. Luminosity recorded outside of these periods is included.

4.1.2 Temperature corrections

The leakage current depends on the temperature of the sensor [48]. The following equation converts the leakage current of a sensor measured at temperature T to that at a reference temperature T_R:

$$I_{\text{leak}}(T_R) = I_{\text{leak}}(T)\left(\frac{T_R}{T}\right)^2 \exp\left[-\frac{E_{\text{eff}}}{2k_B}\left(\frac{1}{T_R} - \frac{1}{T}\right)\right],$$

where E_{eff} is the effective silicon band-gap energy after irradiation, also called the activation energy, and k_B is the Boltzmann constant. A value of 1.21 eV was used for E_{eff} for all sensors studied in

---

[3]This is not the only way to incorporate time-dependence in the thermal history. Another proposal is to sum the inverse temperatures [43]. Such a method has been compared with eq. (3.2) and results in similar predictions for the leakage current at the present fluence levels and annealing times.

ref. [49]. This choice provides consistency when comparing results from different subdetectors. A study using this value, performed with sensors that have been subjected to different radiation conditions, is presented in the next section.

4.2 Optimal $E_{\rm eff}$ study with the silicon sensors on the pixel layers and disks

Dedicated temperature scans were used to measure $E_{\rm eff}$ in the pixel detector. The upper panel of the left plot in figure 2 shows the measured temperature as a function of time during the scan for a representative module in the IBL. The bottom panel shows the measured leakage current and corrections to a reference temperature of 0 °C with several values of $E_{\rm eff}$. The optimal value of $E_{\rm eff}$ in the temperature correction equation is the value that results in corrected leakage current data that best fit a line of zero slope. The best fit is determined using a minimum-χ^2 figure of merit. The optimal $E_{\rm eff}$ is 1.26 eV for this particular module and corresponds to an integrated luminosity of 161 fb^{-1} delivered to the IBL. This procedure is repeated for all modules in the pixel detector and the extracted values of $E_{\rm eff}$ are shown in the right plot of figure 2. The $E_{\rm eff}$ values for the IBL modules were extracted using temperature scan data in Feb. 2018 (May 2019) corresponding to 95 (161) fb^{-1}. The $E_{\rm eff}$ values for all other layers correspond to the temperature scan data in May 2019 and 191 fb^{-1} accumulated in Run 1 and Run 2. The bin ranges of the outer layers are determined by the paired-module powering scheme of module power supplies.

The measured $E_{\rm eff}$ is found to vary by layer, with a small radial dependence. The Layer-2 values are most consistent with 1.21 eV, with slightly lower values observed for Layer-1 and the B-Layer. Higher values of $E_{\rm eff}$ are observed for the IBL. The data are consistent with a small ($O(1\%)$) increase in $E_{\rm eff}$ between 2018 and 2019 for the IBL. It is possible that $E_{\rm eff}$ depends on the composition of irradiating particles, the thermal history, or the sensor doping properties. Further investigations are left to future studies.

The largest uncertainty in the $E_{\rm eff}$ measurement is due to the offset between the measured and true sensor temperatures. This offset is not well-constrained; a ±2 °C uncertainty is used for illustration purposes, acting as a conservative estimate to show the effects of such a shift on the final measurements. In comparison, the statistical uncertainty is found to be negligible. In principle, one could simultaneously extract the temperature offset and $E_{\rm eff}$ from the fit. The $\Delta\chi^2$ landscape is presented in figure 3 and shows that there is a near degeneracy between the extracted temperature offset and $E_{\rm eff}$. Therefore, additional studies of the temperature offset using simulations or laboratory tests will be required to determine $E_{\rm eff}$ with more precision.

4.3 Innermost pixel layer (IBL)

Each sensor is equipped with a negative temperature coefficient (NTC) thermistor for measuring the temperature. On the FEI4 readout chips [50] bonded to the sensors, there is a 10-bit analog-to-digital converter associated with an 8-to-1 analogue multiplexer that can be used to select and read out the temperature, power supply voltages, voltage references, detector leakage current, and other detector control system analogue voltages. The leakage currents were measured at the nominal operational temperature and bias voltage settings. In particular, the temperature started at -2 °C and the high voltage for the planar (3D) sensors started at −80 V (−20 V) at the beginning of 2015 and was subsequently increased to ensure full depletion. The high voltage was increased to −150 V
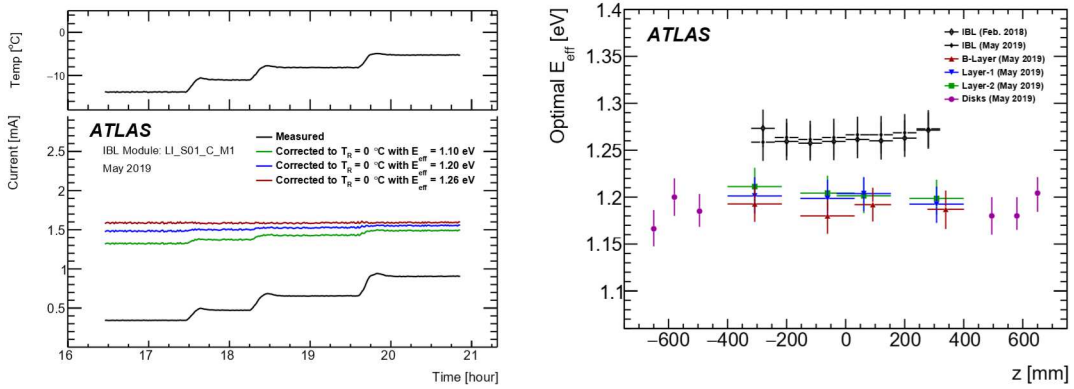
Figure 2. Left: the best value of the effective silicon band-gap energy (E_{eff}) for use in normalizing silicon sensor leakage current to a temperature other than that at which it was recorded is investigated, for one module on the IBL. The top panel shows the temperature of the pixel detector module as set to several fixed values, and measured with the module temperature sensor. The lower panel shows the leakage current data as measured (black line) with a clear temperature dependence. Right: the optimal E_{eff} value is determined for each module and then the average value is computed in bins of z for each layer and disk. The vertical error bars represent the impact on the optimal E_{eff} value due to a ± 2 °C conservative uncertainty in the module temperature. Variations larger than this would be inconsistent with thermal models. Each bin is defined according to the average position of the modules whose data are used.
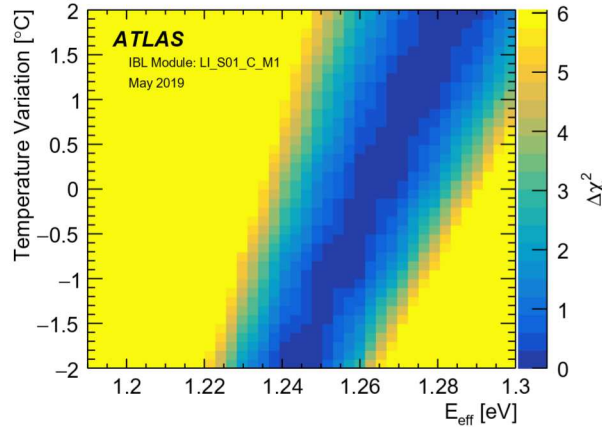
Figure 3. The χ^2 figure of merit is determined for a range of E_{eff} values and variations of the module temperature data, for one module on the IBL. Steps of 0.01 eV, in the range 0.5 eV to 1.5 eV, for E_{eff} (a reduced range is shown for this model) and steps of 0.1 °C, in the range -2.0 °C to 2.0 °C, for the temperature variation are investigated independently. Here the definition of variation is the measured module temperature plus or minus a constant that corresponds to a systematic uncertainty in the temperature sensor reading. The measurement corresponds to data of integrated luminosity 161 fb^{-1} delivered to the IBL.

(-20 V) for the planar (3D) sensors at the end of 2016 corresponding to about 35 fb^{-1}, to -350 V (-40 V) in mid-2017 at about 45 fb^{-1}, and then to -400 V (-40 V) in 2018 at about 95 fb^{-1}. The temperature changed to 10 °C during the first HV increase and then to -13 °C during the second HV increase.

During shutdown periods (such as year-end technical stops), the modules were powered off and no on-sensor temperature reading was available. The cooling during these periods is determined with measurements from the nearby cooling pipes.

The uncertainty in the extracted fluence is dominated by a conservative 10% uncertainty that accounts for the possible difference between the leakage current at the operational bias voltage and the current at the full depletion voltage. After irradiation, there is also an increase in leakage current with increasing bias voltage after full depletion, whereas the Hamburg Model predicts a constant leakage current above the full depletion voltage. Therefore, the choice of voltage for the leakage current measurement is important for comparison with the Hamburg Model prediction. Uncertainties due to the annealing model (0.1%) and data fit (0.5%) are subdominant.

4.3.1 Results

Measurements and scaled predictions averaged over the azimuthal angle ϕ and within module groups are presented in figure 4. The large drops in the current correspond to periods of annealing during year-end technical stops. Apart from an overall constant offset, the model predictions agree with the data within about 10% across Run 2. Despite this good agreement, past 40 fb^{-1} there is a clear monotonic trend in the ratio of the prediction to the data. Judging from the structure in the data and prediction at the start of 2018 (around 95 fb^{-1}), the effects of annealing seem more pronounced in data than in the predictions.

Prior to 40 fb^{-1}, the planar sensors were slightly below full depletion. This can be seen most clearly in figure 5, which presents ratios of the leakage current in the planar sensors to the leakage current in the 3D sensors on the IBL. Ratios of leakage currents are proportional to the ratio of the corresponding predicted fluences if the sensors are fully depleted. The ratio is relatively constant past 40 fb^{-1}, but there is a clear decrease in the ratio between 15 and 35 fb^{-1}. The 3D sensors require a much lower high voltage to be fully depleted and so assuming they are fully depleted during this period, the upper panel of figure 5 displays a measure of the depleted volume.[4] Once the high voltage was increased from −80 V to −150 V, the ratio of the planar sensor to 3D sensor leakage currents stabilized.

4.4 Outer pixel layers and disks

4.4.1 Measurement subsystems

Leakage current data are collected using two independent subsystems, the per-module high-voltage patch panel subsystem (HVPP4) and the multi-module power supply subsystem used to confirm and augment the HVPP4 measurement. The HVPP4 serves as a fan-out point for the bias voltages delivered to the pixel modules from the Iseg high-voltage power supplies [51] and monitors leakage currents at the pixel-module granularity level by means of a Current Monitoring Board system. Further details of the HVPP4 system can be found in ref. [52].

During Run 1, each power supply channel was used to power and read out six or seven modules in parallel. During the long shutdown of the LHC between 2013 and 2015, more power supply units were installed for use in the pixel detector. During LHC Run 2, each power supply channel supplied one or two modules. The sum of the leakage current values is measured for the modules

---

[4]The ratio is predicted to be proportional to the depleted volume up to corrections that are induced by overdepletion.
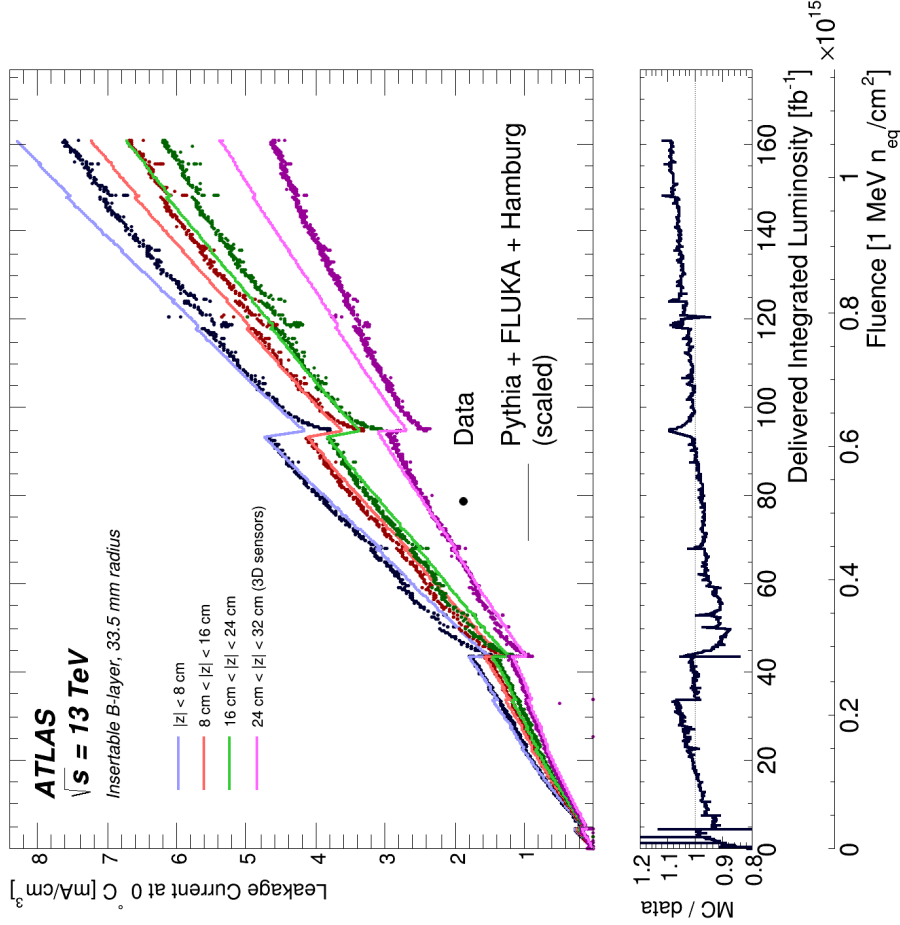
Figure 4. The measured and predicted leakage currents for sensors on the Insertable *B*-layer, both normalized to 0 °C for four module groups spanning $|z| < 8$ cm, 8 $< |z| < 16$ cm, 16 $< |z| < 24$ cm, and 24 $< |z| < 32$ cm. Modules in the highest $|z|$ region use 3D sensors. The A and C sides of the detector ($z > 0$ and $z < 0$) are consistent with each other and averaged. The dominant time-independent uncertainty of 10% is not included to avoid overlapping bands. The prediction is based on the thermal history of the modules combined with the Hamburg Model for modelling changes in the leakage current and PYTHIA + FLUKA for simulating the overall fluence. For all four predictions, the overall scale normalization is based on a fit to the data across the entire range. Normalization factors are determined per $|z|$ region. The lower panel shows the ratio of the prediction to the data for the innermost module group. Similar MC/data trends are observed for the other three $|z|$ regions. For illustration, the fluence is shown as a lower horizontal axis using the nominal luminosity-to-fluence from simulation at $|z| = 0$.

supplied by a common power supply unit. The precision of measurements of the leakage current read with the power supply units was improved during LHC Run 2. The raw leakage current data measured by both the HVPP4 system and the power supplies are stored in the COOL database [53].

Leakage currents were measured for each module individually using the HVPP4 subsystem in LHC Run 1 and Run 2 and for pairs of modules using the power supply subsystem in LHC Run 2. These measurements are subsequently averaged for each barrel layer and each disk. Averaged binned measurements are also examined for ϕ and z dependence for a more refined investigation of the spatial dependence of the radiation damage.
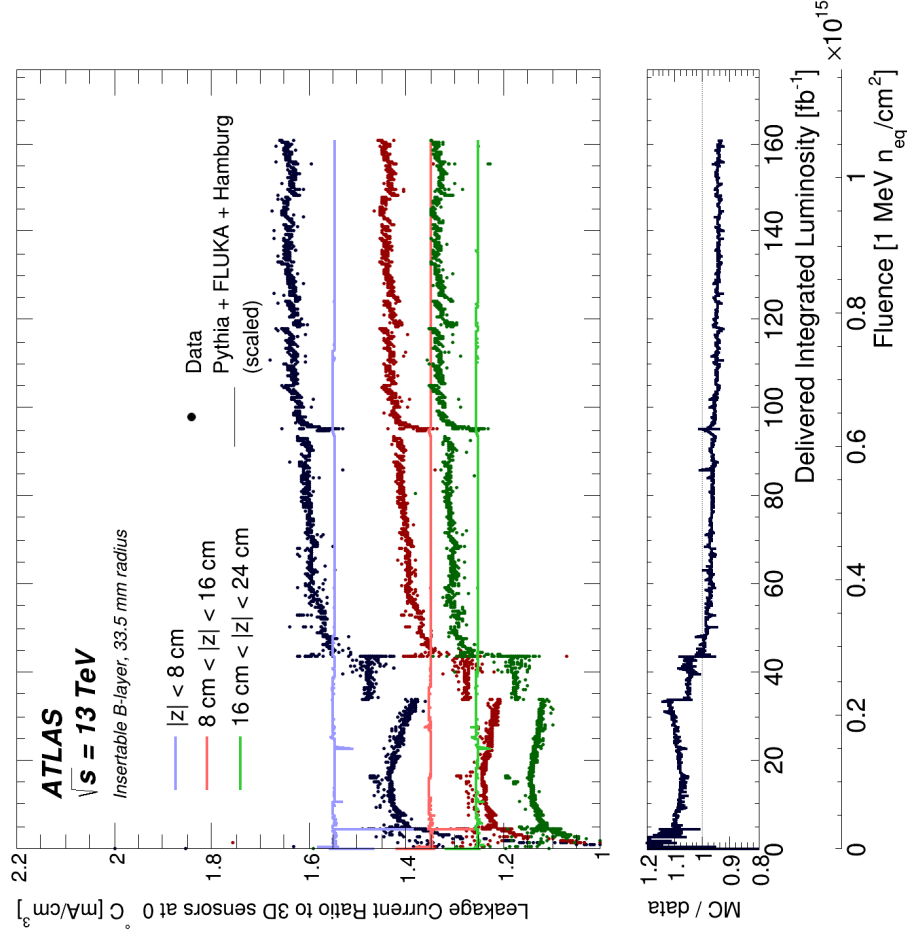
Figure 5. The measured and predicted leakage currents on the Insertable *B*-layer, both normalized to 0 °C, divided by the currents in the 3D modules at 24 < |z| < 32 cm. The other three module groups represent |z| < 8 cm, 8 < |z| < 16 cm, and 16 < |z| < 24 cm. The A and C sides of the detector ($z > 0$ and $z < 0$) are consistent with each other and averaged. The dominant time-independent uncertainty of 10% is not included to avoid overlapping bands. The prediction is based on the thermal history of the modules combined with the Hamburg Model for modelling changes in the leakage current and PYTHIA + FLUKA for simulating the overall fluence. For all four predictions, the overall scale normalization is based on a fit to the data across the entire range. Normalization factors are determined per |z| region. The lower panel shows the ratio of the prediction to the data for the innermost module group. Similar MC/data trends are observed for the other three |z| regions. For illustration, the fluence is shown as a lower horizontal axis using the nominal luminosity-to-fluence from simulation at |z| = 0.

4.4.2 Precision and systematic uncertainties

This section provides the elements that contribute to the uncertainty of the measurement of the leakage current, the Hamburg Model predictions, and the measurement of the fluence. The two subsystems, HVPP4 and the power supplies, are used to make independent measurements; the final uncertainty for each subsystem is calculated by adding all contributing elements (described below) in quadrature. The statistical uncertainty is used in the fit, over the full temporal range of the measurement, to determine a scale factor needed to bring the Hamburg Model into agreement

with the data. The precision of current measurements made with the HVPP4 current monitoring circuit contributes a 12% uncertainty. The precision of current measurements made with the power supply units contributes 4% to the total measurement uncertainty [51]. The current measurements are made approximately once per minute and that interval contributes a 0.5% uncertainty; this uncertainty is calculated by investigating the changes in the data over 10-minute intervals — a time interval over which the leakage current is not expected to change. The precision of the temperature measurements contributes a 2.9% uncertainty; the temperature is also not expected to fluctuate over short time intervals and is thus calculated in the same way as the current uncertainty. Uncertainties due to a possible difference between the temperature of the point on the module at which the temperature is measured and the point on the silicon sensor to which the temperature is attributed are found to be 10% through changes to the modelled leakage current when a difference in temperature of $1\,^\circ$C is applied. The total uncertainty of the leakage current data collected with HVPP4 is determined by adding in quadrature the HVPP4 current monitoring circuit measurement uncertainty, the current measurement uncertainty, and each of the two temperature uncertainties; the HVPP4 data uncertainty is found to be 15.9%. The total uncertainty of the leakage current data collected with the dual-module power supply units is determined by adding in quadrature the power supply precision uncertainty, the current measurement uncertainty, and each of the two temperature uncertainties; the power supply data uncertainty is found to be 11.2%.

4.4.3 Results

Measurements of leakage currents in all three barrel layers from February 2011 (early in LHC operation) to November 2018 are shown in figure 6. The B-Layer (red points) shows the highest leakage current consistently. Layer-1 (blue points) and Layer-2 (green points) have progressively lower levels. Measurements on each layer are averaged over a representative sample of modules in z and ϕ. The measurements are consistent with expected higher levels of radiation for sensors closer to the interaction point. The Hamburg Model predictions have been scaled to match the measured leakage current with a luminosity-to-fluence scaling factor applied for each layer. The scale factors are determined in four z-binned regions for each layer. The average of the scaled Hamburg Model predictions in each is used in a comparison with the average leakage current data. After the application of the scale factors, the Hamburg Model predictions fit well to the data throughout the full period of the measurement. The leakage current data are normalized to $0\,^\circ$C; the average module temperature is shown in the top panel. Leakage current data are shown for periods of operation when the high voltage is applied across the silicon sensor; the average module bias voltage is shown in the middle panel of figure 6. Some spikes in the bias voltage are visible starting near the end of 2017, corresponding to bias voltage scans. Bias voltage scans prior to 2017 are not shown in the figure. Some dates corresponding to extended periods when the LHC beams were off, resulting in annealing of the sensors, are displayed within the lower panel with grey vertical lines. Not all such periods are marked. The module temperatures are taken to be $18\,^\circ$C during these shutdown periods. During part of LS1, from February 2013 to February 2014 (LS1 ended in April 2015), the pixel detector was removed from the ATLAS cavern and kept at $22\,^\circ$C.

The slopes of the leakage current plots in figure 6 is due to constant damage from the applied fluence, and a slight difference is observed between data and prediction near the end of Run 2. The drops in the leakage current are due to annealing; the annealing can also change the overall
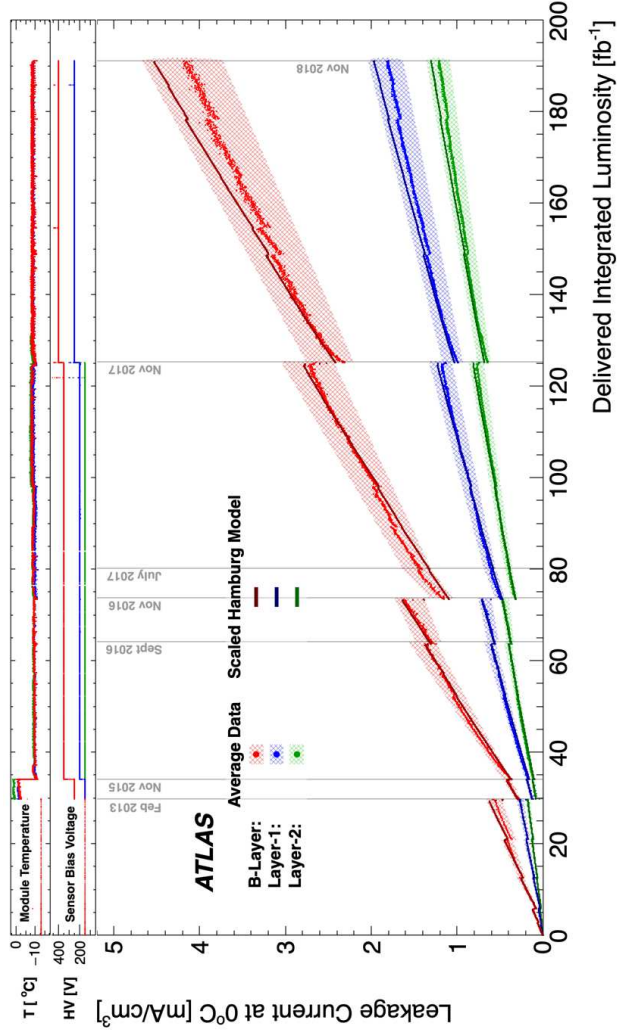
Figure 6. Average measured leakage current of a representative sample of modules on the *B*-Layer, Layer-1 and Layer-2 over the full period of operation. The scaled prediction from the Hamburg Model is also shown. The bands include uncertainties on the measurement, as described in section 4.4.2.

shape as a function of integrated luminosity. The observed differences are accounted for in the uncertainty bands, which are dominated by a temperature bias. Other sources of uncertainty such as the luminosity uncertainty ($O(1\%)$) are subdominant.

To reveal the impact of constant damage, a study of the ratios of the leakage currents across the layers is performed. Measured ratios of the average leakage current for modules on the *B*-Layer to the average leakage current for modules on Layer-2, and of the average leakage current for modules on Layer-1 to the average leakage current of modules on Layer-2, are shown in figure 7 for LHC Run 2. These ratios are, as predicted, fairly constant as a function of integrated luminosity. Once again, some dates corresponding to extended periods when the LHC beams were off are displayed with grey vertical lines. Also shown in figure 7 are the ratios of the unscaled Hamburg Model predictions for LHC Run 2. The vertical axis is proportional to the ratio of the applied fluences. The fluence of one layer relative to other layers is well predicted without the need for scale factors.

4.5   Strip detector and disks

The ATLAS SCT consists of 4088 modules of silicon-strip detectors: 2112 in the barrel region, and 988 per endcap region, EC-A or EC-C. The barrel modules are mounted on four cylindrical supports and named as Barrels 3 to 6 (B3 to B6 for short). Each endcap has nine disks (labelled 1 to 9), each consisting of up to three rings of modules. The rings, in order of increasing radius, are named *Inner*, *Middle* and *Outer*.
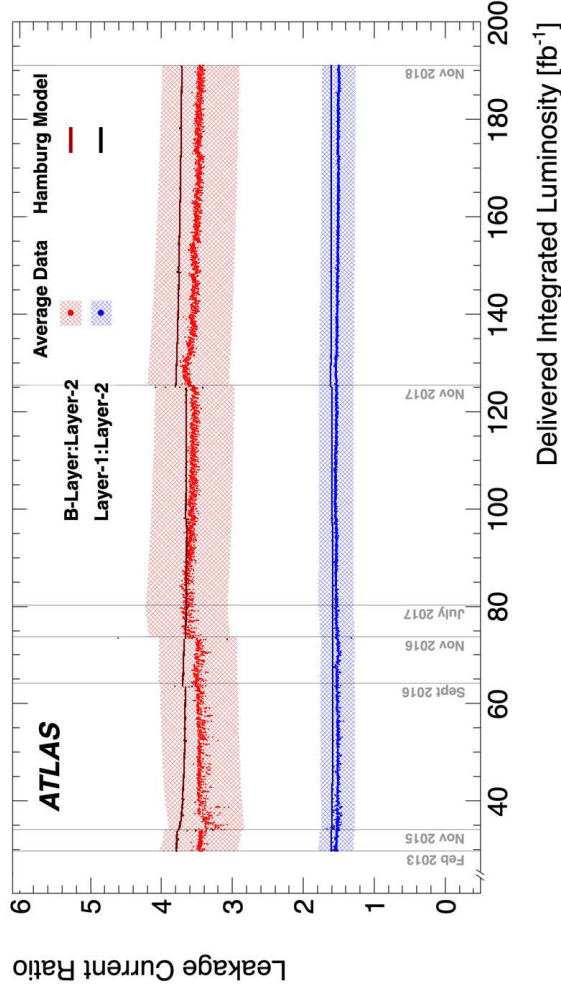
Figure 7. Ratios of the *B*-Layer and Layer-1 leakage current data to Layer-2 leakage current for the LHC Run 2 period of ATLAS operation. The bands include uncertainties on the measurement, as described in section 4.4.2

4.5.1 Temperature measurement

Each barrel module consists of four rectangular silicon-strip sensors. Two sensors on each side are daisy-chained together. Two sides of identical pairs are glued back-to-back with a 380 μm thick anisotropic thermal pyrolytic graphite (TPG) substrate in between.

The endcap region has four module types and five different trapezoid-shaped sensors. Modules in the *Outer* and *Middle* rings consist of two daisy-chained sensors on each side, whereas those in the *Inner* ring have one sensor per side. A TPG spine sandwiched between two sensor sides conducts heat away from the sensors to the cooling block contacts. The modules in the *Outer* and *Middle* are supported and cooled by their contacts with two cooling blocks; the main block is shared between the hybrid and the spine, while the far block cools only the spine. Inner modules are cooled only through the main block.

SCT modules are cooled using the inner detector's evaporative C_3F_8 cooling system [54]. Each loop cools 48 (up to 33) barrel (endcap) modules. A total of 44 and 72 cooling loops are operated simultaneously for the barrel and endcap regions, respectively. The cooling-pipe temperatures were set to about $-12\,°C$, $-7\,°C$, $-13\,°C$ and $-10\,°C$ in B3–B5, B6, EC-A and EC-C, respectively. The cooling temperatures for B6 were set higher because of a failure in resistive pad heaters on the thermal enclosure cylinders at the SCT-TRT interface. There is a 3 °C difference in the cooling temperature settings of EC-A and EC-C due in part to different assembly sites. The initial cooling temperature settings were kept from 2009 to 2018 except for 6 months during 2015 to avoid condensation in the SCT volumes.

The sensor temperature T_{sensor} of each module is deduced from a hybrid-board temperature T_{hybrid} measured by NTC thermistors mounted on the hybrid circuit board. A temperature offset between T_{hybrid} and T_{sensor} strongly depends on the mechanical and thermal structure. It also differs

module-by-module due to slightly different thermal resistances of the hybrid-circuit, sensor and cooling pipe. The temperature offset is determined by measuring the hybrid temperature and the leakage current of the sensors with and without power applied to the hybrid low voltage (LV). The hybrid temperature and the leakage current data are collected at several cooling temperature settings. The temperature differences are extracted by an interpolation of leakage currents vs T_{hybrid} curves. The offsets are similar to predictions from the thermal finite-element method. The individual differences are 3–5 °C and 12–20 °C in barrel and endcap modules, respectively. The offsets of the B6 modules are not measured because the TRT would become too cold at the SCT-TRT interface if the LV power were not supplied to the B6 modules.

During long shutdowns in winters and LS1, as well as occasional power-cut cases, T_{hybrid} data are not available. In most cases, however, the temperature monitors of the evaporative cooling system were active. Since there was no heat generation in the SCT volume, the temperature of the closest cooling pipe could be used as an estimate of T_{sensor}, which occasionally reached as high as 20 °C.

The precision of the T_{hybrid} measurement is determined by using temperature data (when all HVs and LVs are off) from the two thermistors mounted on each side of a barrel module. These readings agree well with a root-mean-square (RMS) uncertainty of 0.27 °C. A major uncertainty in T_{hybrid} comes from the smallest digitization unit of 0.33 °C used in the conversion from thermistor resistance to temperature. However, module-by-module fluctuations in the leakage currents cause larger spreads and thus such digitization effects smear out once the mean of >30 modules belonging to the same module group is taken.

4.5.2 Time evolution of leakage current

All voltages and currents of the HV power supplies, as well as T_{hybrid}, were continuously monitored and stored in a database called the Detector Control System Data Viewer [55]. For the leakage current of each module, typically 150 data points of leakage current are recorded every hour because of the presence of small ripples of about 0.2%. During a physics run lasting several hours, as the instantaneous luminosity goes down, the HV current drops by 0.2–2% (values in late 2018, none in Run 1) due to sensor self-heating. A simple time-weighted average during each physics run is taken for the present study.

Another way to get the leakage current data is to read the leakage current mean values recorded in the gain calibration runs. In-beam leakage current averages are consistent with the mean values from nearby calibration run values within 1%.

It should be noted that the leakage current depends on the HV applied to the sensor. Well above the full depletion voltage, the leakage current increases by several percent per 100 V. In addition, due to the filter resistance of about 12 kΩ in the HV supply lines, the true voltage on the sensor could be 20 V less in the worst case for B3 modules in late 2018, introducing up to 1% additional uncertainty in the leakage current measurement.

Figure 8 shows the time evolution of the leakage current during the Run 2 period including winter shutdowns for four representative module groups, two each from barrel and endcap regions. The top plots show the histories of the estimated sensor temperatures T_{sensor}, which were around −1 °C, +5 °C and −7 °C for B3, B6 and both EC-A and EC-C, respectively, during the running periods, and were >15 °C during LS1 and the winter shutdowns. In the 2015 beam time, all modules

except those in B6 were set warmer to avoid a condensation risk in the SCT volume. The HV is adjusted to always be above the prediction for full depletion. The second set of plots from the top in figure 8 display normalized leakage currents, and the third and fourth sets of plots display ratios of data to predictions from the Hamburg Model and the Sheffield Model[5] [56, 57]. Uncertainties from the model predictions are shown with bands which are calculated by varying each parameter of the model by 1σ and adding the resulting changes in quadrature. Uncertainties in the temperature measurements (1 °C) and delivered luminosities (3.7%) are also included.

The leakage current anneals out by 20–30% during each winter shutdown, as evident from the drop in the current during periods of no beam. The Sheffield Model systematically predicts 15% more leakage current than the Hamburg Model. For most of the cases, the ratios seldom change by more than 5% during a given year, which is good evidence for the leakage current being proportional to irradiation with good-enough short annealing terms. Any year-by-year dependencies in the ratios may be due to the influence of insufficiently accurate estimates of T_{sensor} during shutdowns or model limitations or both on annealing effects.

4.5.3 Lateral distribution of leakage current

Figures 9(a) and 9(b) show leakage currents for all barrel and endcap modules, respectively, as of November 2018 with the applied HV set to 150 V. In these plots, modules with the same r and z locations but different azimuthal angles are bundled side by side. Modules of EC-A and EC-C are coloured differently, as are modules built with sensors from different manufacturers. Permanently disabled modules (42 in total out of about 2000) are not displayed in the plot. It can be seen that almost all modules in the same group have quite similar leakage currents with a spread of about 3%. Despite the difference of 2–3 °C between the EC-A and EC-C cooling temperatures, the leakage currents agree well once they are normalized to 0 °C.

Additional differences between sensors across the detector did not result in appreciable variations among the leakage currents. The majority of the modules are constructed from silicon wafers with crystal lattice orientation (Miller indices) $\langle 111 \rangle$ while a small number of modules in the barrel use wafers with $\langle 100 \rangle$ lattice orientation. The barrel sensors and 75% of the endcap sensors were supplied by Hamamatsu Photonics (HPK)[6] while the remaining endcap sensors were supplied by CiS.[7] Sensors supplied by the two manufacturers meet the same performance specifications, but differ in design and processing details [11]. The CiS sensors for EC inner modules were oxygen-enriched. No appreciable differences in leakage current were observed among sensors from different manufacturers (HPK vs CiS), or different crystal orientations ($\langle 111 \rangle$ vs $\langle 100 \rangle$) or standard/oxygen-enriched silicon materials. One sees a clear and systematic trend of higher leakage currents in higher rapidity regions at all radii covered by the SCT. In the barrel layers, the normalized leakage currents in near-centre modules are about 3% smaller than in edge modules at $|z| = 68$ cm.

---

[5]This is an alternative to the Hamburg Model that has been developed for the ATLAS strip detector. While the Hamburg model uses an exponential combined with a logarithmic function, the Sheffield model is based on a sum of five exponentials. The parameters of these exponentials were tuned to SCT-like modules prior to the start of the LHC. While it has not yet been compared with pixel data from any experiment, this will be important for the future (see section 5.1).

[6]Hamamatsu Photonics Co. Ltd.,1126–1 Ichino-cho, Hamamastu, Shizuoka 431-3196, Japan.

[7]CiS Institut für Mikrosensorik gGmbH, Konrad-Zuse-Strasse 14, 99099 Erfurt, Germany.
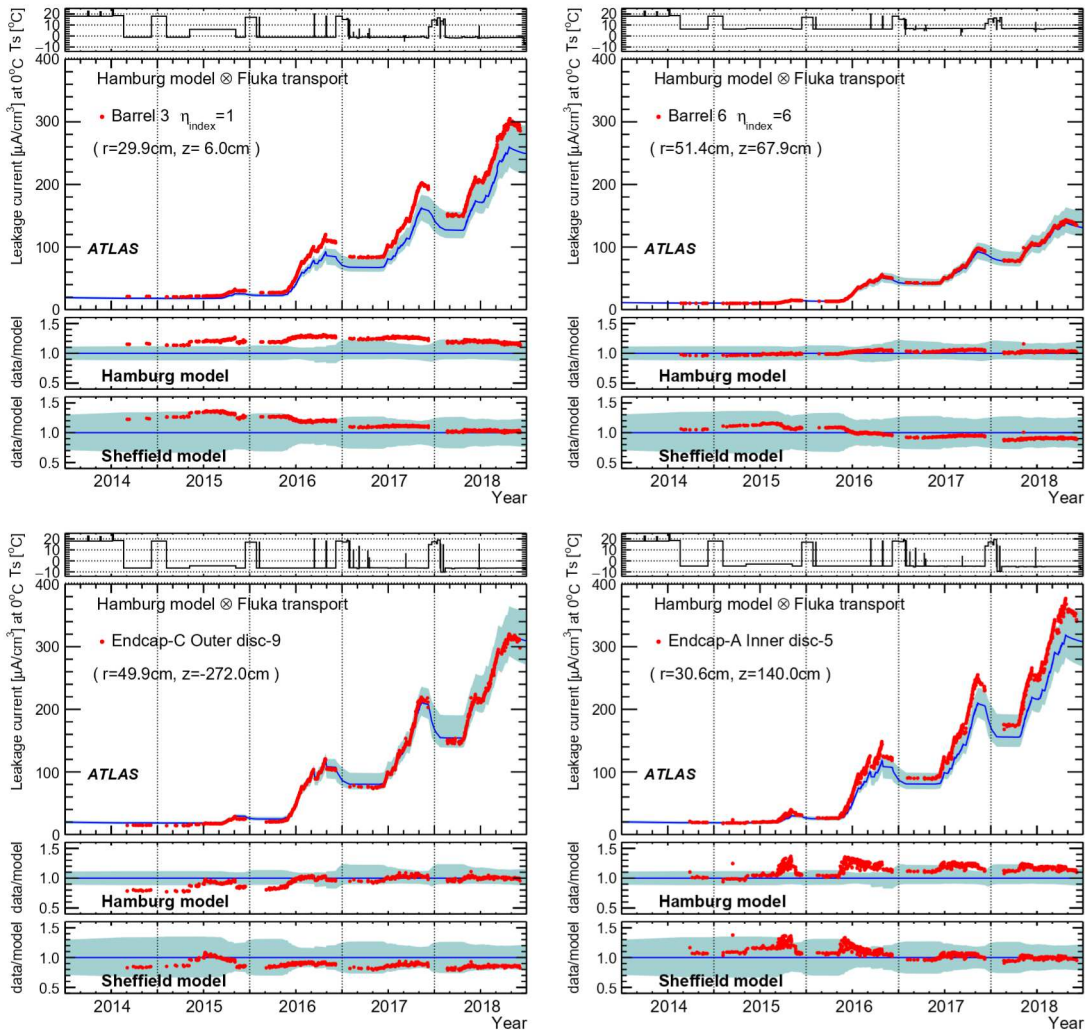
Figure 8. Typical time evolution of normalized leakage currents in the four SCT modules groups, one each from B3, B6, EC-C and EC-A regions. Top plots show histories of deduced sensor temperatures, while the second plots are leakage current data and Hamburg Model predictions. Each data point represents an average of time-weighted leakage current means over 30–56 modules in a single physics or calibration run. The two bottom plots show the ratios of data to predictions from the Hamburg and Sheffield models, using the same conversion factors as in FLUKA transport simulations. Coloured bands show 1σ uncertainties of the model predictions.

This is in contrast to the observation at the end of Run 1 when a slight excess was seen in the central B3 layer but a flat behavior was seen in other barrel layers [9].

The observed gross trends are reproduced fairly well by the Hamburg Model times the conversion factors from FLUKA or GEANT transport simulations. In general, leakage current predictions are systematically 10–20% higher in the GEANT case. The ratios in modules near the centre of B3 are 10% higher than in those at the edges, but the difference is less in the B6 layer, indicating an additional fluence component close to the interaction point. In the endcap regions, however, the data-to-model ratios are fairly constant for all disks in the range $|z| = 85$ to 270 cm although their

– 17 –

leakage currents being different by up to 50%.

(a)   (b)
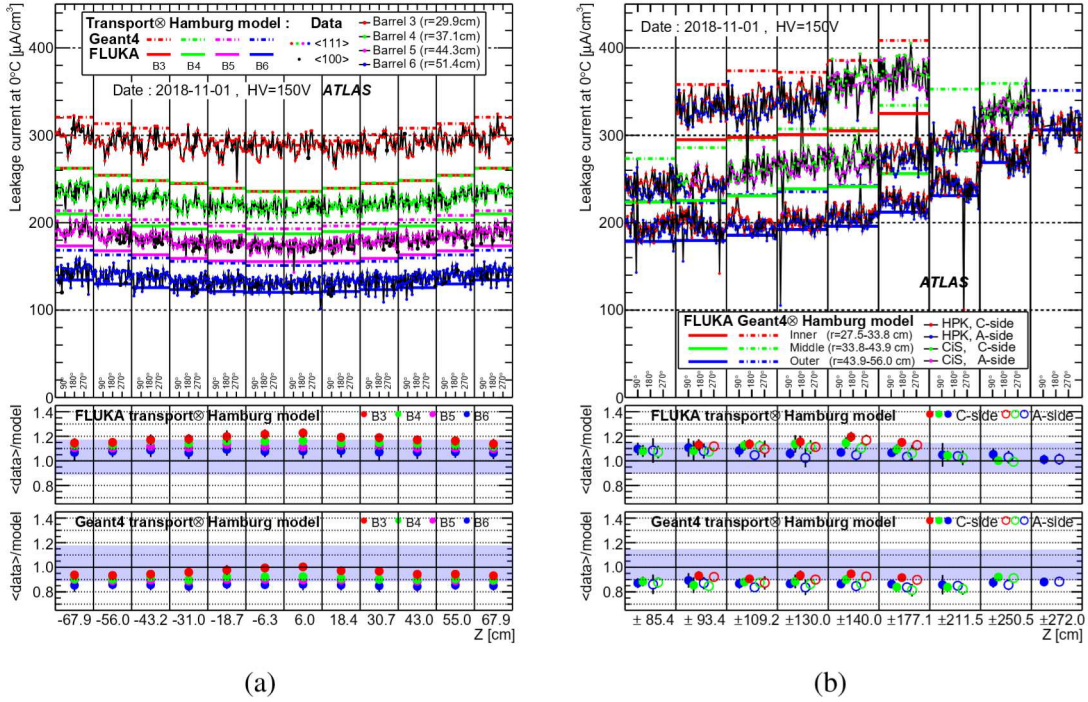
Figure 9. Leakage current measured at HV set to 150 V normalized to 0 °C per unit volume for all (a) barrel modules and (b) endcap modules as of November 1, 2018. At the same r and z location, modules with different ϕ indices are arranged horizontally from left ($\phi = 0°$) to right ($\phi = 360°$). Endcap side-A and side-C as well as sensor manufacturers (Hamamatsu (HPK) and CiS) are plotted in different colours. Horizontal solid/dot-dash bars indicate model predictions of the Hamburg Model using the conversion factors by FLUKA (solid) / GEANT (dot-dash) transport simulations. In the two ratio plots, mean and RMS values via Gaussian fits of modules belonging to the same group are plotted. The model uncertainties are shown by blue bands.

5   Leakage current and fluence comparisons

This section incorporates measurements and simulations for all of the silicon-based inner-detector subsystems described in the previous sections. For leakage current comparisons, the measurements are presented from the end of Run 2. The simulations are combined with the thermal and luminosity history of the various sensors to transform fluence predictions to leakage current predictions for all detector regions. For fluence comparisons, the annealing models are used to fit a scale factor that normalizes the fluence in the simulations per detector region. The nominal predicted fluence combined with the scale factor gives the measured fluence rate, Φ/L_{int} (from eq. 3.1).

Figure 10 presents a comparison of the measured leakage current and fluence rate for both the pixel and strip detectors. The leakage current is the value at the end of Run 2 while the fluence rate is independent of time.[8] The fluence rate prediction agrees well with the IBL data at $|z| = 0$

---

[8]This is exactly true for the IBL, but for the other layers, a minor model dependence is introduced by using the relative total cross sections between collision energies (lower in Run 1 than in Run 2) to be able to measure a single value. About 85% of the data come from Run 2, which further reduces the impact of this correction.

and with all the SCT data. In contrast, there is a much stronger $|z|$-dependence observed in the IBL data than is predicted (numerical values are presented in table 1) and the overall fluence is significantly higher than predicted for the outer pixel layers. Near the centre of the detector, the measured fluence is 30–50% higher than predicted by the simulation. For Layer-1 and Layer-2, the difference is 30–40%. For the IBL, the measured fluence at $|z| = 30$ cm is about 50% of the value at $|z| = 0$. These data are presented as a function of η instead of z in figure 11. The trends are exactly the same as in figure 10, but now the $|\eta| < 2.5$ acceptance of the silicon tracking detector is clear. The fluence on the inner layers is mostly determined by the primary charged-pion flux, which is relatively constant as a function of η. In contrast, a significant fraction of the fluence in the outer layers of the SCT is due to neutrons that are produced by interactions with material in the dense regions of the ATLAS calorimeters.

The data are presented in a third way in figure 12, demonstrating the radial dependence of the measured leakage current and fluence. The fluence drops off approximately as the square of the inverse radius, with deviations resulting from particles produced through interactions with the detector. Beyond the pixel detector, the FLUKA and GEANT4 simulations bracket the measured values.

The ratio of the simulated values to the leakage current data, as shown in figure 12, is presented in table 2. The values in this table provide concrete input for further studies of the radiation environment at the LHC.

Table 1. IBL scale factors as a function of z, depicted in figure 10. The measurements are consistent between $+z$ and $-z$ and the predictions are symmetric by construction, so the values are presented in bins of $|z|$.

z Bin	Mean SF
32 cm > $|z|$ > 24 cm	0.56 ± 0.06
24 cm > $|z|$ > 16 cm	0.77 ± 0.08
16 cm > $|z|$ > 8 cm	0.84 ± 0.09
8 cm > $|z|$ > 0 cm	0.97 ± 0.10

Table 2. Mean, minimum, and maximum simulation-to-data ratios (scale factors, SF) for each barrel layer in the inner detector, as depicted in figure 12. The average uncertainty in the ratio is in the rightmost column.

Detector	Layer	r [cm]	Mean SF	Min. SF	Max. SF	SF uncert.
	IBL	3.30	0.78	0.56	0.97	0.08
Pixel	B-Layer	5.10	1.28	1.11	1.47	0.15
	Layer-1	8.90	1.31	1.19	1.44	0.15
	Layer-2	12.30	1.39	1.32	1.46	0.16
	Barrel 3	29.90	1.13	1.11	1.17	0.11
SCT	Barrel 4	37.10	1.09	1.05	1.15	0.11
	Barrel 5	44.30	1.06	1.01	1.13	0.10
	Barrel 6	51.40	1.03	0.98	1.09	0.11

5.1 Discussion

The leakage current is a powerful probe of bulk damage in silicon caused by irradiation, and the results in the previous section indicate areas where simulations provide an excellent description of the data as well as other areas where there are significant deviations from observations. The purpose of this section is to examine possible sources of the differences between data and simulation, including systematic effects for which there is currently no concrete uncertainty model. Differences could be due to a variety of sources, affecting both the data measurements and simulation predictions:

Method biases in the measurement. In theory, the current should rise, plateau, and then rise again as the high voltage is increased from zero up through breakdown. In practice, the current increases past full depletion for irradiated sensors so there is no unique high voltage at which to determine the leakage current. Changes in the current past full depletion are typically small ($O(10\%)$) but not negligible for the current level of measurement precision. Furthermore, as remarked earlier, the current depends strongly on temperature. This presents a challenge because the temperature of the sensors is often not known precisely. Temperature measurements are also complicated by bulk heat generation. This affects both the leakage current measurements and their interpretation because the measured temperature is used as an input for leakage current normalization and leakage current predictions. A coupled complication is that the effective band-gap energy E_{eff} may not be constant, as noted in section 4.2. Additional measurements with other observables such as the Lorentz angle, depletion voltage, charge collection efficiency, etc. may add valuable information to confirm the trends observed with the leakage current.

Physics modelling for the outgoing particle spectra. The input to radiation damage model predictions is the type and energy of particles produced by the primary proton-proton collisions. The physics of soft quantum chromodynamics governs the majority of particles produced and these dynamics are not well understood. A variety of models exist, as do measurements of the total inelastic cross section [58–60] and minimum-bias / underlying-event spectra [61–63]. Systematic studies of model uncertainties and data/simulation differences may provide insight into deviations observed in the leakage current measurement.

Transport models. Most of the significant data/prediction differences are common to both FLUKA and GEANT4. An important difference between the two transport models is that GEANT4 includes a more detailed description of the ATLAS detector geometry. Improvements in the description of the inner-detector material may mitigate discrepancies, but the material is known precisely from studies of secondary interactions [64].

Damage factors. The largest single (largely unknown) uncertainty comes from the damage factors. These factors have been tabulated by the RD50 Collaboration [22–26] and are based on a combination of measurements and simulations. A key challenge is that there are not many beam facilities with monochromatic beams of hadrons in the relevant energy range. Furthermore, the damage from neutrons changes rapidly near 1 MeV so there is a significant uncertainty when converting from the damage from pions to the damage from neutrons. Improving the precision of these factors is challenging, but a first important step would be to estimate their uncertainty.

Annealing models. The Hamburg Model is the community standard for leakage current modelling. Aside from the overall luminosity-to-fluence conversion, it has achieved excellent precision over the full lifetime of the LHC. However, there may be early indications from the pixel data that there are systematic differences between the model and data and these may grow to become significant in the future. Alternative models are available, such as the Sheffield Model [56, 57]. Comparisons with this model as well as updating/tuning the Hamburg Model (including how to model periods of non-constant temperature) may be necessary for describing the leakage currents when including Run 3 and the high-luminosity phase of the LHC.

Despite these challenges, the leakage current is an important tool that will continue to improve in its descriptive and predictive power with additional studies on various fronts described above.

Figure 10. The leakage current at the end of Run 2 (left) and the fluence rate (right) as a function of z for the silicon-based parts of the ATLAS inner detector. The predicted values are symmetric in z by construction. Distances given in parentheses after layer names correspond to the radial positions of the sensors relative to the geometric centre of ATLAS. For the IBL, the error bars are dominated by the residual dependence of the leakage current on the high voltage past full depletion; for the outer layers of the pixel detector, the uncertainty is dominated by a power supply uncertainty and uncertainties in the temperature and luminosity; for the SCT, the uncertainty is due to the sensor temperature, the luminosity, and the sensor thickness (for fluence) and the RMS spread across modules (leakage current). Uncertainties in the silicon damage factors (relevant for the simulation and the Hamburg Model) are not included.

Figure 11. The leakage current at the end of Run 2 (left) and the fluence rate (right) as a function of η for the silicon-based parts of the ATLAS inner detector. The predicted values are symmetric in η by construction. Distances given in parentheses after layer names correspond to the radial positions of the sensors relative to the geometric centre of ATLAS. For the IBL, the error bars are dominated by the residual dependence of the leakage current on the high voltage past full depletion; for the outer layers of the pixel detector, the uncertainty is dominated by a power supply uncertainty and uncertainties in the temperature and luminosity; for the SCT, the uncertainty is due to the sensor temperature, the luminosity, and the sensor thickness (for fluence) and the RMS spread across modules (leakage current). Uncertainties in the silicon damage factors (relevant for the simulation and the Hamburg Model) are not included.
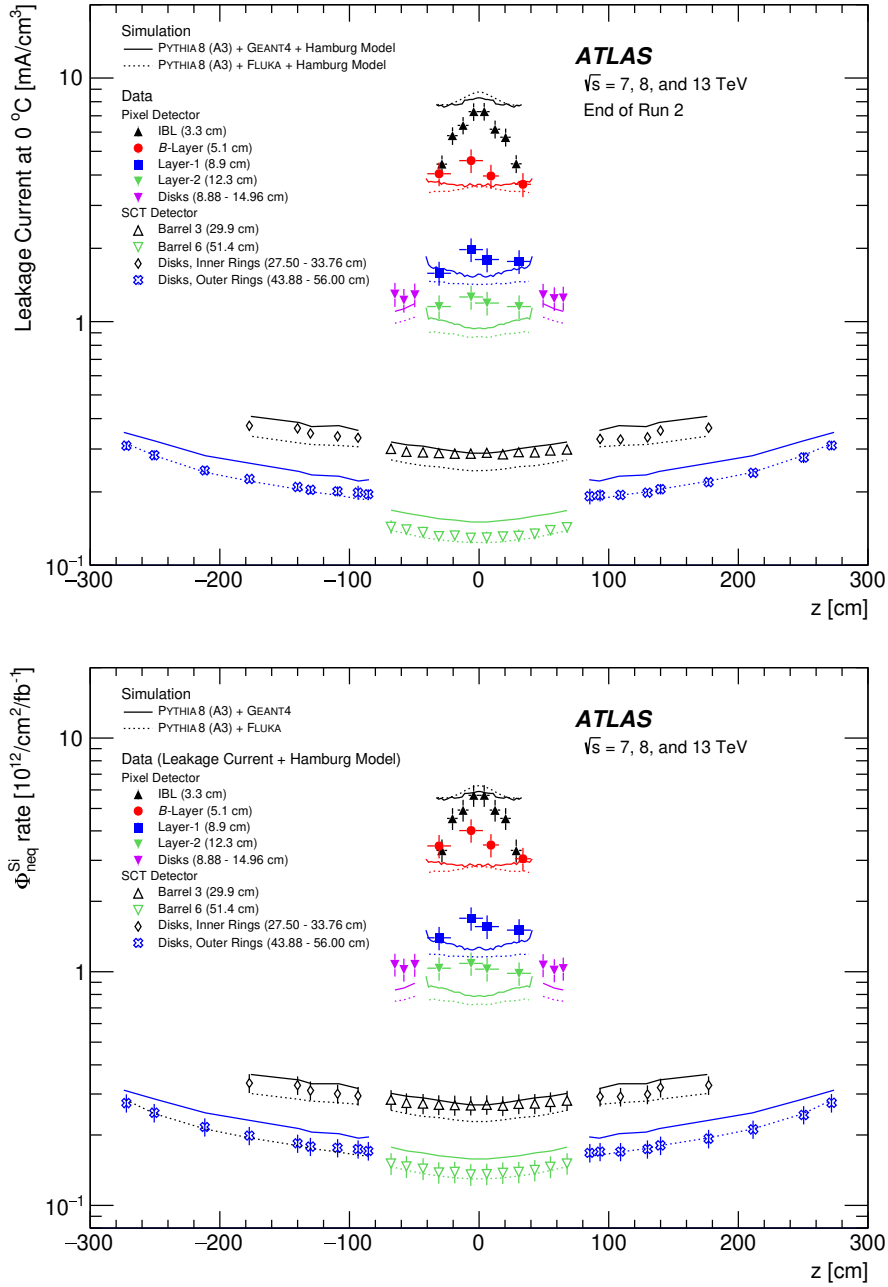
Figure 12. The leakage current at the end of Run 2 (left) and the fluence rate (right) as a function of radius for the silicon-based parts of the ATLAS inner detector. The length of the horizontal bands representing the simulation is chosen to aid the comparison with data — the actual radial uncertainty from the finite size of the sensors is comparable to the marker sizes. For the IBL, the error bars are dominated by the residual dependence of the leakage current on the high voltage past full depletion; for the outer layers of the pixel detector, the uncertainty is dominated by a power supply uncertainty and uncertainties in the temperature and luminosity; for the SCT, the uncertainty is due to the sensor temperature, the luminosity, and the sensor thickness (for fluence) and the RMS spread across modules (leakage current). Uncertainties in the silicon damage factors (relevant for the simulation and the Hamburg Model) are not included.
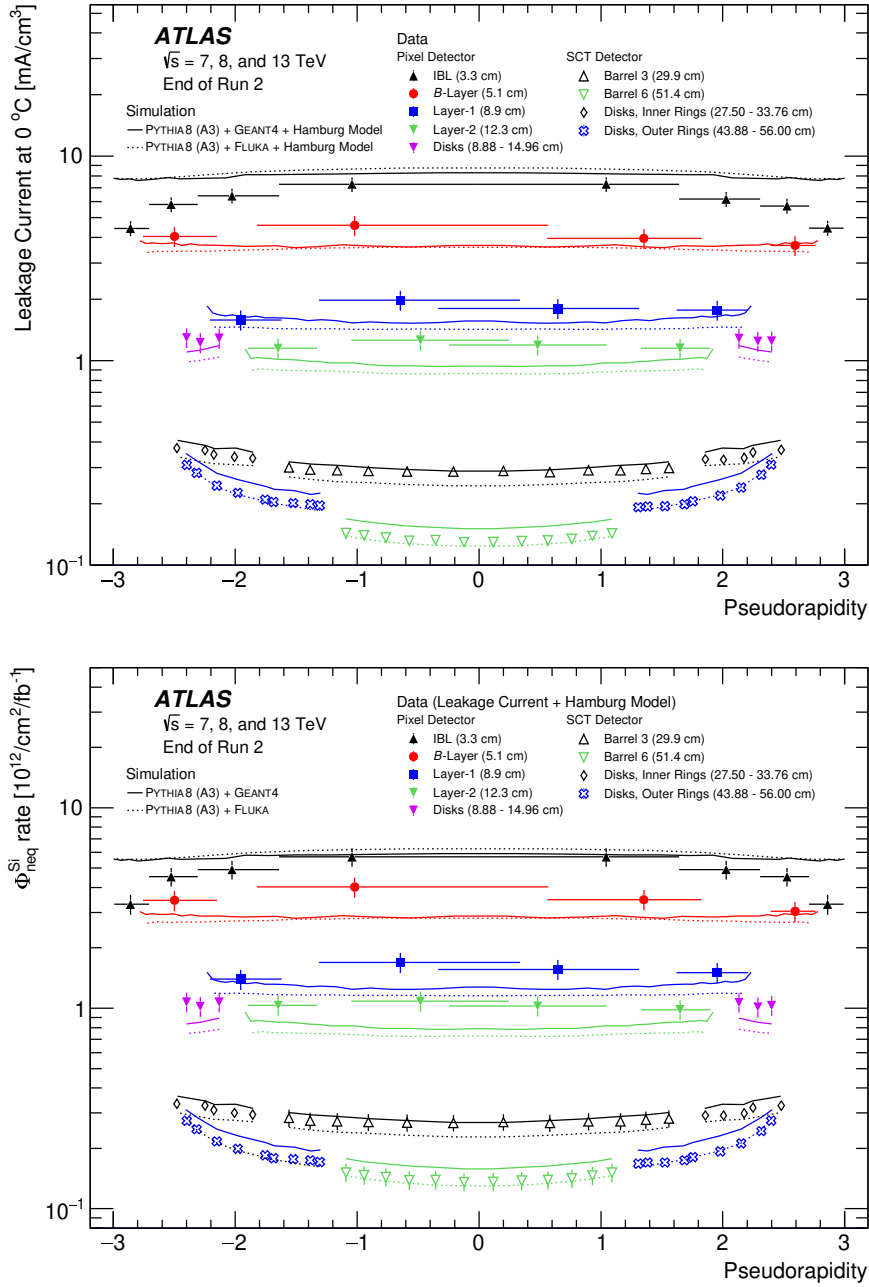
6 Conclusions and outlook

This paper presents a measurement of the sensor leakage current for all the silicon detectors in the ATLAS tracking detector. Over time and position within the detector, the existing models provide a reasonable description of the data. Two significant discrepancies have been observed: there is a stronger $|z|$ dependence in the innermost layers than predicted by simulations and the overall fluence appears to be up to 50% higher than in simulation for the intermediate layers between 5 cm and 15 cm from the collision point. Overall, the fluence delivered to the innermost layer of the pixel detector is about 10^{15} 1 MeV n_{eq}/cm^2 while the innermost portion of the SCT detector has experienced about 6×10^{13} 1 MeV n_{eq}/cm^2. The damage caused by these fluences has degraded the detector performance, but continued monitoring and modelling will support development of operational and offline analysis strategies to mitigate the impact on the physics output of the experiment. Sensors designed for the high-luminosity phase of the LHC will need to cope with about an order of magnitude more fluence, and the investigations presented here will provide valuable input to preparations for those data-taking conditions in the near future.

Acknowledgments

PIC (Spain), ASGC (Taiwan), RAL (U.K.) and BNL (U.S.A.), the Tier-2 facilities worldwide and large non-WLCG resource providers. Major contributors of computing resources are listed in ref. [65].

References

[1] ATLAS collaboration, *The ATLAS Experiment at the CERN Large Hadron Collider*, 2008 *JINST* **3** S08003.

[2] ATLAS collaboration, *Modelling radiation damage to pixel sensors in the ATLAS detector*, 2019 *JINST* **14** P06012 [arXiv:1905.03739].

[3] G. Aad et al., *ATLAS pixel detector electronics and sensors*, 2008 *JINST* **3** P07007.

[4] ATLAS Collaboration, *Atlas insertable b-layer technical design report*, CERN-LHCC-2010-013, ATLAS-TDR-19, addendum: CERN-LHCC-2012-009; ATLAS-TDR-19-ADD-1.

[5] ATLAS IBL collaboration, *Production and Integration of the ATLAS Insertable B-Layer*, 2018 *JINST* **13** T05008 [arXiv:1803.00844].

[6] ROSE collaboration, *3rd RD48 status report*, Tech. Rep. CERN-LHCC-2000-009, CERN, Geneva (Dec, 1999).

[7] ROSE collaboration, *Developments for radiation hard silicon detectors by defect engineering - Results by the CERN RD48 (ROSE) Collaboration*, *Nucl. Instrum. Meth. A* **465** (2000) 60.

[8] S.I. Parker, C.J. Kenney and J. Segal, *3-D: A New architecture for solid state radiation detectors*, *Nucl. Instrum. Meth. A* **395** (1997) 328.

[9] ATLAS collaboration, *Operation and performance of the ATLAS semiconductor tracker*, 2014 *JINST* **9** P08009 [arXiv:1404.7473].

[10] A. Abdesselam et al., *The barrel modules of the ATLAS semiconductor tracker*, *Nucl. Instrum. Meth. A* **568** (2006) 642.

[11] A. Ahmad et al., *The Silicon microstrip sensors of the ATLAS semiconductor tracker*, *Nucl. Instrum. Meth. A* **578** (2007) 98.

[12] ATLAS collaboration, *The ATLAS semiconductor tracker end-cap module*, *Nucl. Instrum. Meth. A* **575** (2007) 353.

[13] M. Moll, *Radiation damage in silicon particle detectors: Microscopic defects and macroscopic propertie*, Ph.D. thesis, Hamburg University, Hamburg, Germany (1999), http://www-library.desy.de/cgi-bin/showprep.pl?desy-thesis99-040.

[14] THE ROSE COLLABORATION collaboration, *The NIEL scaling hypothesis applied to neutron spectra of irradiation facilities and in the ATLAS and CMS SCT*, ROSE/TN/97-2 (1997).

[15] T. Sjöstrand, S. Mrenna and P.Z. Skands, *PYTHIA 6.4 Physics and Manual*, *JHEP* **05** (2006) 026 [hep-ph/0603175].

[16] T. Sjöstrand et al., *An introduction to PYTHIA 8.2*, *Comput. Phys. Commun.* **191** (2015) 159 [arXiv:1410.3012].

[17] A.D. Martin, W.J. Stirling, R.S. Thorne and G. Watt, *Parton distributions for the LHC*, *Eur. Phys. J. C* **63** (2009) 189 [arXiv:0901.0002].

[18] ATLAS collaboration, *The PYTHIA 8 A3 tune description of ATLAS minimum bias and inelastic measurements incorporating the Donnachie-Landshoff diffractive model*, Tech. Rep. ATL-PHYS-PUB-2016-017, CERN, Geneva (Aug, 2016).

[19] G. Battistoni et al., *The FLUKA code: Description and benchmarking*, *AIP Conf. Proc.* **896** (2007) 31.

[20] A. Ferrari, P.R. Sala, A. Fassò and J. Ranft, *FLUKA: A multi-particle transport code (program version 2005)*, CERN-2005-010, INFN-TC-2005-11, SLAC-R-773, CERN, Geneva (2005).

[21] GEANT4 collaboration, *GEANT4–a simulation toolkit*, *Nucl. Instrum. Meth. A* **506** (2003) 250.

[22] G.P. Summers, E.A. Burke, P. Shapiro, S.R. Messenger and R.J. Walters, *Damage correlations in semiconductors exposed to gamma, electron and proton radiations*, *IEEE Trans. Nucl. Sci.* **40** (1993) 1372.

[23] M. Huhtinen and P.A. Aarnio, *Pion induced displacement damage in silicon devices*, *Nucl. Instrum. Meth. A* **335** (1993) 580.

[24] A. Konobeyev, Y. Korovin and V. Sosnin, *Neutron displacement cross-sections for structural materials below 800 mev*, *J. Nucl. Mater.* **186** (1992) 117.

[25] P.J. Griffin, J.G. Kelly, T.F. Luera and J. VanDenburg, *Snl rml recommended dosimetry cross section compendium*, SAND92-0094 (1993).

[26] M. Moll, *Displacement damage in silicon detectors for high energy physics*, *IEEE Trans. Nucl. Sci.* **65** (2018) 1561.

[27] G. Battistoni et al., *Overview of the FLUKA code*, *Annals Nucl. Energy* **82** (2015) 10.

[28] T.T. Böhlen et al., *The FLUKA Code: Developments and Challenges for High Energy and Medical Applications*, *Nucl. Data Sheets* **120** (2014) 211.

[29] *Fluka web page*, (2014), https://fluka.cern.

[30] A. Capella, U. Sukhatme, C.-I. Tan and J. Tran Thanh Van, *Dual parton model*, *Phys. Rept.* **236** (1994) 225.

[31] A. Ferrari and P.R. Sala, *The Physics of High Energy Reactions*, in proceedings of *Workshop on Nuclear Reaction Data and Nuclear Reactors Physics, Design and Safety*, International Centre for Theoretical Physics, Miramare-Trieste, Italy, (1997) p. 424, ATL-PHYS-97-113, ATL-GE-PN-113.

[32] A. Ferrari and P.R. Sala, *A new model for hadronic interactions at intermediate-energies for the FLUKA code*, in *International Conference on Monte Carlo Simulation in High-Energy and Nuclear Physics*, MC 93 Tallahassee, Florida, 22–26 February 1993, pp. 277–288.

[33] A. Fassò, A. Ferrari, J. Ranft and P.R. Sala, *FLUKA: performances and applications in the intermediate energy range*, in proceedings of *AEN/NEA Specialists' Meeting on Shielding Aspects of Accelerators, Targets and Irradiation Facilities*, Arlington, Texas, U.S.A., 28–29 April 1994, pp. 287–304, https://cds.cern.ch/record/2724814.

[34] A. Ferrari, P.R. Sala, J. Ranft and S. Roesler, *The Production of residual nuclei in peripheral high-energy nucleus-nucleus interactions*, *Z. Phys. C* **71** (1996) 75 [nucl-th/9603010].

[35] A. Ferrari, P.R. Sala, J. Ranft and S. Roesler, *Cascade particles, nuclear evaporation, and residual nuclei in high-energy hadron - nucleus interactions*, *Z. Phys. C* **70** (1996) 413 [nucl-th/9509039].

[36] B. Andersson, G. Gustafson and B. Nilsson-Almqvist, *A Model for Low p_T Hadronic Reactions, with Generalizations to Hadron - Nucleus and Nucleus-Nucleus Collisions*, *Nucl. Phys. B* **281** (1987) 289.

[37] B. Andersson, A. Tai and B.-H. Sa, *Final state interactions in the (nuclear) FRITIOF string interaction scenario*, *Z. Phys. C* **70** (1996) 499.

[38] B. Nilsson-Almqvist and E. Stenlund, *Interactions Between Hadrons and Nuclei: The Lund Monte Carlo, Fritiof Version 1.6*, *Comput. Phys. Commun.* **43** (1987) 387.

[39] B. Ganhuyag and V. Uzhinsky, *Modified FRITIOF code: negative charged particle production in high energy nucleus–nucleus interactions*, *Czech. J. Phys.* **47** (1997) 913.

[40] J. Boudreau and V. Tsulaia, *The GeoModel Toolkit for Detector Description*, *Computing in High Energy Physics and Nuclear Physics* (2004) 353.

[41] ATLAS collaboration, *The ATLAS Simulation Infrastructure*, *Eur. Phys. J. C* **70** (2010) 823 [arXiv:1005.4568].

[42] J.-C. Beyer, *Optimisation of pixel modules for the ATLAS inner tracker at the high-luminosity LHC*, Ph.D. thesis, Munich U., 2019. 10.5282/edoc.23939.

[43] CMS collaboration, *Measurement of the bulk leakage current of silicon sensors of the CMS preshower after an integrated luminosity of 6.17 fb^{-1}, at $\sqrt{s}$ = 7 TeV*, 2013 *JINST* **8** P02004.

[44] ATLAS collaboration, *Luminosity determination in pp collisions at $\sqrt{s}$ = 8 TeV using the ATLAS detector at the LHC*, *Eur. Phys. J. C* **76** (2016) 653 [arXiv:1608.03953].

[45] S. van der Meer, *Calibration of the effective beam height in the ISR*, Tech. Rep. CERN-ISR-PO-68-31, ISR-PO-68-31, CERN, Geneva (1968).

[46] ATLAS collaboration, *Luminosity determination in pp collisions at $\sqrt{s}$ = 13 TeV using the ATLAS detector at the LHC*, Tech. Rep. ATLAS-CONF-2019-021, CERN, Geneva (Jun, 2019).

[47] G. Avoni et al., *The new LUCID-2 detector for luminosity measurement and monitoring in ATLAS*, 2018 *JINST* **13** P07017.

[48] CERN-ROSE/RD48 collaboration, *Leakage current of hadron irradiated silicon detectors - material dependence*, *Nucl. Instrum. Meth. A* **426** (1999) 87.

[49] A. Chilingarov, *Temperature dependence of the current generated in si bulk*, 2013 *JINST* **8** P10003.

[50] M. Garcia-Sciveres et al., *The FE-I4 pixel readout integrated circuit*, *Nucl. Instrum. Meth. A* **636** (2011) S155.

[51] Iseg Spezialelektronik GmbH, *High Voltage Power Supply EHQ F607n-F, Operators Manual*, https://iseg-hv.com.

[52] *A Leakage Current-based Measurement of the Radiation Damage in the ATLAS Pixel Detector*, Tech. Rep. ATL-INDET-PUB-2014-004, CERN, Geneva (Aug, 2014).

[53] A. Valassi, R. Basset, M. Clemencic, G. Pucciani, S.A. Schmidt and M. Wache, *COOL, LCG conditions database for the LHC experiments: Development and deployment status*, *2008 IEEE Nucl. Sci. Symp. Conf. R.* (2008) 3021.

[54] D. Attree et al., *The evaporative cooling system for the ATLAS inner detector*, 2008 *JINST* **3** P07003.

[55] C. Tsarouchas, S. Schlenker, G. Dimitrov and G. Jahn, *DCS Data Viewer, an Application that Accesses ATLAS DCS Historical Data*, *J. Phys. Conf. Ser.* **513** (2014) 032097.

[56] R.S. Harper et al., *Evolution of silicon microstrip detector currents during proton irradiation at the CERN PS*, *Nucl. Instrum. Meth. A* **479** (2002) 548.

[57] R. Harper, *Radiation damage studies of silicon detectors and searching for an intermediate mass Higgs boson at ATLAS*, thesis CERN-THESIS-2001-083, (Oct, 2001).

[58] ATLAS collaboration, *Measurement of the Inelastic Proton-Proton Cross Section at √s = 13 TeV with the ATLAS Detector at the LHC*, *Phys. Rev. Lett.* **117** (2016) 182002 [arXiv:1606.02625].

[59] CMS collaboration, *Measurement of the inelastic proton-proton cross section at √s = 13 TeV*, *JHEP* **07** (2018) 161 [arXiv:1802.02613].

[60] LHCb collaboration, *Measurement of the inelastic pp cross-section at a centre-of-mass energy of 13 TeV*, *JHEP* **06** (2018) 100 [arXiv:1803.10974].

[61] ATLAS collaboration, *Charged-particle distributions at low transverse momentum in √s = 13 TeV pp interactions measured with the ATLAS detector at the LHC*, *Eur. Phys. J. C* **76** (2016) 502 [arXiv:1606.01133].

[62] ATLAS collaboration, *Measurement of charged-particle distributions sensitive to the underlying event in √s = 13 TeV proton-proton collisions with the ATLAS detector at the LHC*, *JHEP* **03** (2017) 157 [arXiv:1701.05390].

[63] CMS collaboration, *Pseudorapidity distribution of charged hadrons in proton-proton collisions at √s = 13 TeV*, *Phys. Lett. B* **751** (2015) 143 [arXiv:1507.05915].

[64] ATLAS collaboration, *Study of the material of the ATLAS inner detector for Run 2 of the LHC*, 2017 *JINST* **12** P12009 [arXiv:1707.02826].

[65] ATLAS collaboration, *ATLAS Computing Acknowledgements*, Tech. Rep. ATL-SOFT-PUB-2020-001, CERN, Geneva (May, 2020).

The ATLAS collaboration

G. Aad[101], B. Abbott[127], D.C. Abbott[102], A. Abed Abud[36], K. Abeling[53], D.K. Abhayasinghe[93],
S.H. Abidi[29], O.S. AbouZeid[40], N.L. Abraham[155], H. Abramowicz[160], H. Abreu[159], Y. Abulaiti[6],
A.C. Abusleme Hoffman[145a], B.S. Acharya[66a,66b,o], B. Achkar[53], L. Adam[99], C. Adam Bourdarios[5],
L. Adamczyk[83a], L. Adamek[165], J. Adelman[120], A. Adiguzel[12c,ad], S. Adorni[54], T. Adye[142],
A.A. Affolder[144], Y. Afik[159], C. Agapopoulou[64], M.N. Agaras[38], A. Aggarwal[118], C. Agheorghiesei[27c],
J.A. Aguilar-Saavedra[138f,138a,ac], A. Ahmad[36], F. Ahmadov[79], W.S. Ahmed[103], X. Ai[46], G. Aielli[73a,73b],
S. Akatsuka[85], M. Akbiyik[99], T.P.A. Åkesson[96], E. Akilli[54], A.V. Akimov[110], K. Al Khoury[39],
G.L. Alberghi[23b,23a], J. Albert[174], M.J. Alconada Verzini[160], S. Alderweireldt[36], M. Aleksa[36],
I.N. Aleksandrov[79], C. Alexa[27b], T. Alexopoulos[10], A. Alfonsi[119], F. Alfonsi[23b,23a], M. Alhroob[127],
B. Ali[140], S. Ali[157], M. Aliev[164], G. Alimonti[68a], C. Allaire[36], B.M.M. Allbrooke[155], P.P. Allport[21],
A. Aloisio[69a,69b], F. Alonso[88], C. Alpigiani[147], E. Alunno Camelia[73a,73b], M. Alvarez Estevez[98],
M.G. Alviggi[69a,69b], Y. Amaral Coutinho[80b], A. Ambler[103], L. Ambroz[133], C. Amelung[36], D. Amidei[105],
S.P. Amor Dos Santos[138a], S. Amoroso[46], C.S. Amrouche[54], C. Anastopoulos[148], N. Andari[143],
T. Andeen[11], J.K. Anders[20], S.Y. Andrean[45a,45b], A. Andreazza[68a,68b], V. Andrei[61a], C.R. Anelli[174],
S. Angelidakis[9], A. Angerami[39], A.V. Anisenkov[121b,121a], A. Annovi[71a], C. Antel[54], M.T. Anthony[148],
E. Antipov[128], M. Antonelli[51], D.J.A. Antrim[18], F. Anulli[72a], M. Aoki[81], J.A. Aparisi Pozo[172],
M.A. Aparo[155], L. Aperio Bella[46], N. Aranzabal[36], V. Araujo Ferraz[80a], C. Arcangeletti[51], A.T.H. Arce[49],
J-F. Arguin[109], S. Argyropoulos[52], J.-H. Arling[46], A.J. Armbruster[36], A. Armstrong[169], O. Arnaez[165],
H. Arnold[36], Z.P. Arrubarrena Tame[113], G. Artoni[133], H. Asada[116], K. Asai[125], S. Asai[162], N.A. Asbah[59],
E.M. Asimakopoulou[170], L. Asquith[155], J. Assahsah[35e], K. Assamagan[29], R. Astalos[28a], R.J. Atkin[33a],
M. Atkinson[171], N.B. Atlay[19], H. Atmani[64], P.A. Atmasiddha[105], K. Augsten[140], V.A. Austrup[180],
G. Avolio[36], M.K. Ayoub[15c], G. Azuelos[109,ak], D. Babal[28a], H. Bachacou[143], K. Bachas[161],
F. Backman[45a,45b], P. Bagnaia[72a,72b], H. Bahrasemani[151], A.J. Bailey[172], V.R. Bailey[171], J.T. Baines[142],
C. Bakalis[10], O.K. Baker[181], P.J. Bakker[119], E. Bakos[16], D. Bakshi Gupta[8], S. Balaji[156],
R. Balasubramanian[119], E.M. Baldin[121b,121a], P. Balek[178], F. Balli[143], W.K. Balunas[133], J. Balz[99],
E. Banas[84], M. Bandieramonte[137], A. Bandyopadhyay[19], L. Barak[160], W.M. Barbe[38], E.L. Barberio[104],
D. Barberis[55b,55a], M. Barbero[101], G. Barbour[94], K.N. Barends[33a], T. Barillari[114], M-S. Barisits[36],
J. Barkeloo[130], T. Barklow[152], B.M. Barnett[142], R.M. Barnett[18], Z. Barnovska-Blenessy[60a],
A. Baroncelli[60a], G. Barone[29], A.J. Barr[133], L. Barranco Navarro[45a,45b], F. Barreiro[98],
J. Barreiro Guimarães da Costa[15a], U. Barron[160], S. Barsov[136], F. Bartels[61a], R. Bartoldus[152],
G. Bartolini[101], A.E. Barton[89], P. Bartos[28a], A. Basalaev[46], A. Basan[99], A. Bassalat[64,ah], M.J. Basso[165],
C.R. Basson[100], R.L. Bates[57], S. Batlamous[35f], J.R. Batley[32], B. Batool[150], M. Battaglia[144],
M. Bauce[72a,72b], F. Bauer[143,*], P. Bauer[24], H.S. Bawa[31], A. Bayirli[12c], J.B. Beacham[49], T. Beau[134],
P.H. Beauchemin[168], F. Becherer[52], P. Bechtle[24], H.P. Beck[20,q], K. Becker[176], C. Becot[46], A.J. Beddall[12a],
V.A. Bednyakov[79], C.P. Bee[154], T.A. Beermann[180], M. Begalli[80b], M. Begel[29], A. Behera[154], J.K. Behr[46],
J.F. Beirer[53,36], F. Beisiegel[24], M. Belfkir[5], G. Bella[160], L. Bellagamba[23b], A. Bellerive[34], P. Bellos[21],
K. Beloborodov[121b,121a], K. Belotskiy[111], N.L. Belyaev[111], D. Benchekroun[35a], N. Benekos[10],
Y. Benhammou[160], D.P. Benjamin[6], M. Benoit[29], J.R. Bensinger[26], S. Bentvelsen[119], L. Beresford[133],
M. Beretta[51], D. Berge[19], E. Bergeaas Kuutmann[170], N. Berger[5], B. Bergmann[140], L.J. Bergsten[26],
J. Beringer[18], S. Berlendis[7], G. Bernardi[134], C. Bernius[152], F.U. Bernlochner[24], T. Berry[93], P. Berta[46],
A. Berthold[48], I.A. Bertram[89], O. Bessidskaia Bylund[180], S. Bethke[114], A. Betti[42], A.J. Bevan[92],
S. Bhatta[154], D.S. Bhattacharya[175], P. Bhattarai[26], V.S. Bhopatkar[6], R. Bi[137], R.M. Bianchi[137],
O. Biebel[113], R. Bielski[36], K. Bierwagen[99], N.V. Biesuz[71a,71b], M. Biglietti[74a], T.R.V. Billoud[140],
M. Bindi[53], A. Bingul[12d], C. Bini[72a,72b], S. Biondi[23b,23a], C.J. Birch-sykes[100], G.A. Bird[21,142],
M. Birman[178], T. Bisanz[36], J.P. Biswal[3], D. Biswas[179j], A. Bitadze[100], C. Bittrich[48], K. Bjørke[132],
T. Blazek[28a], I. Bloch[46], C. Blocker[26], A. Blue[57], U. Blumenschein[92], G.J. Bobbink[119],

V.S. Bobrovnikov[121b,121a], D. Bogavac[14], D. Bogdanchikov[121b,121a], C. Bohm[45a], V. Boisvert[93],
P. Bokan[170,53], T. Bold[83a], M. Bomben[134], M. Bona[92], J.S. Bonilla[130], M. Boonekamp[143], C.D. Booth[93],
A.G. Borbély[57], H.M. Borecka-Bielska[109], L.S. Borgna[94], G. Borissov[89], D. Bortoletto[133],
D. Boscherini[23b], M. Bosman[14], J.D. Bossio Sola[103], K. Bouaouda[35a], J. Boudreau[137],
E.V. Bouhova-Thacker[89], D. Boumediene[38], R. Bouquet[134], A. Boveia[126], J. Boyd[36], D. Boye[29],
I.R. Boyko[79], A.J. Bozson[93], J. Bracinik[21], N. Brahimi[60d,60c], G. Brandt[180], O. Brandt[32], F. Braren[46],
B. Brau[102], J.E. Brau[130], W.D. Breaden Madden[57], K. Brendlinger[46], R. Brener[159], L. Brenner[36],
R. Brenner[170], S. Bressler[178], B. Brickwedde[99], D.L. Briglin[21], D. Britton[57], D. Britzger[114], I. Brock[24],
R. Brock[106], G. Brooijmans[39], W.K. Brooks[145d], E. Brost[29], P.A. Bruckman de Renstrom[84], B. Brüers[46],
D. Bruncko[28b], A. Bruni[23b], G. Bruni[23b], M. Bruschi[23b], N. Bruscino[72a,72b], L. Bryngemark[152],
T. Buanes[17], Q. Buat[154], P. Buchholz[150], A.G. Buckley[57], I.A. Budagov[79], M.K. Bugge[132], O. Bulekov[111],
B.A. Bullard[59], T.J. Burch[120], S. Burdin[90], C.D. Burgard[46], A.M. Burger[128], B. Burghgrave[8], J.T.P. Burr[46],
C.D. Burton[11], J.C. Burzynski[102], V. Büscher[99], E. Buschmann[53], P.J. Bussey[57], J.M. Butler[25],
C.M. Buttar[57], J.M. Butterworth[94], W. Buttinger[142], C.J. Buxo Vazquez[106], A.R. Buzykaev[121b,121a],
G. Cabras[23b,23a], S. Cabrera Urbán[172], D. Caforio[56], H. Cai[137], V.M.M. Cairo[152], O. Cakir[4a], N. Calace[36],
P. Calafiura[18], G. Calderini[134], P. Calfayan[65], G. Callea[57], L.P. Caloba[80b], A. Caltabiano[73a,73b],
S. Calvente Lopez[98], D. Calvet[38], S. Calvet[38], T.P. Calvet[101], M. Calvetti[71a,71b], R. Camacho Toro[134],
S. Camarda[36], D. Camarero Munoz[98], P. Camarri[73a,73b], M.T. Camerlingo[74a,74b], D. Cameron[132],
C. Camincher[36], M. Campanelli[94], A. Camplani[40], V. Canale[69a,69b], A. Canesse[103], M. Cano Bret[77],
J. Cantero[128], Y. Cao[171], M. Capua[41b,41a], R. Cardarelli[73a], F. Cardillo[172], G. Carducci[41b,41a], T. Carli[36],
G. Carlino[69a], B.T. Carlson[137], E.M. Carlson[174,166a], L. Carminati[68a,68b], M. Carnesale[72a,72b],
R.M.D. Carney[152], S. Caron[118], E. Carquin[145d], S. Carrá[46], G. Carratta[23b,23a], J.W.S. Carter[165],
T.M. Carter[50], M.P. Casado[14,g], A.F. Casha[165], E.G. Castiglia[181], F.L. Castillo[172], L. Castillo Garcia[14],
V. Castillo Gimenez[172], N.F. Castro[138a,138e], A. Catinaccio[36], J.R. Catmore[132], A. Cattai[36], V. Cavaliere[29],
V. Cavasinni[71a,71b], E. Celebi[12b], F. Celli[133], K. Cerny[129], A.S. Cerqueira[80a], A. Cerri[155], L. Cerrito[73a,73b],
F. Cerutti[18], A. Cervelli[23b,23a], S.A. Cetin[12b], Z. Chadi[35a], D. Chakraborty[120], M. Chala[138f], J. Chan[179],
W.S. Chan[119], W.Y. Chan[90], J.D. Chapman[32], B. Chargeishvili[158b], D.G. Charlton[21], T.P. Charman[92],
M. Chatterjee[20], C.C. Chau[34], S. Chekanov[6], S.V. Chekulaev[166a], G.A. Chelkov[79,af], B. Chen[78],
C. Chen[60a], C.H. Chen[78], H. Chen[15c], H. Chen[29], J. Chen[60a], J. Chen[39], J. Chen[26], S. Chen[135],
S.J. Chen[15c], X. Chen[15b], Y. Chen[60a], Y-H. Chen[46], C.L. Cheng[179], H.C. Cheng[62a], H.J. Cheng[15a],
A. Cheplakov[79], E. Cheremushkina[122], R. Cherkaoui El Moursli[35f], E. Cheu[7], K. Cheung[63],
L. Chevalier[143], V. Chiarella[51], G. Chiarelli[71a], G. Chiodini[67a], A.S. Chisholm[21], A. Chitan[27b], I. Chiu[162],
Y.H. Chiu[174], M.V. Chizhov[79,s], K. Choi[11], A.R. Chomont[72a,72b], Y. Chou[102], Y.S. Chow[119],
L.D. Christopher[33f], M.C. Chu[62a], X. Chu[15a,15d], J. Chudoba[139], J.J. Chwastowski[84], D. Cieri[114],
K.M. Ciesla[84], V. Cindro[91], I.A. Cioară[27b], A. Ciocio[18], F. Cirotto[69a,69b], Z.H. Citron[178,k], M. Citterio[68a],
D.A. Ciubotaru[27b], B.M. Ciungu[165], A. Clark[54], P.J. Clark[50], S.E. Clawson[100], C. Clement[45a,45b],
L. Clissa[23b,23a], Y. Coadou[101], M. Cobal[66a,66c], A. Coccaro[55b], J. Cochran[78], R. Coelho Lopes De Sa[102],
S. Coelli[68a], H. Cohen[160], A.E.C. Coimbra[36], B. Cole[39], J. Collot[58], P. Conde Muiño[138a,138h],
S.H. Connell[33c], I.A. Connelly[57], F. Conventi[69a,al], A.M. Cooper-Sarkar[133], F. Cormier[173], L.D. Corpe[94],
M. Corradi[72a,72b], E.E. Corrigan[96], F. Corriveau[103,aa], M.J. Costa[172], F. Costanza[5], D. Costanzo[148],
G. Cowan[93], J.W. Cowley[32], J. Crane[100], K. Cranmer[124], R.A. Creager[135], S. Crépé-Renaudin[58],
F. Crescioli[134], M. Cristinziani[150], M. Cristoforetti[75a,75b], V. Croft[168], G. Crosetti[41b,41a], A. Cueto[5],
T. Cuhadar Donszelmann[169], H. Cui[15a,15d], A.R. Cukierman[152], W.R. Cunningham[57], S. Czekierda[84],
P. Czodrowski[36], M.M. Czurylo[61b], M.J. Da Cunha Sargedas De Sousa[60b], J.V. Da Fonseca Pinto[80b],
C. Da Via[100], W. Dabrowski[83a], T. Dado[47], S. Dahbi[33f], T. Dai[105], C. Dallapiccola[102], M. Dam[40],
G. D'amen[29], V. D'Amico[74a,74b], J. Damp[99], J.R. Dandoy[135], M.F. Daneri[30], M. Danninger[151], V. Dao[36],
G. Darbo[55b], A. Dattagupta[130], S. D'Auria[68a,68b], C. David[166b], T. Davidek[141], D.R. Davis[49],
I. Dawson[148], K. De[8], R. De Asmundis[69a], M. De Beurs[119], S. De Castro[23b,23a], N. De Groot[118],

P. de Jong[119] , H. De la Torre[106] , A. De Maria[15c] , D. De Pedis[72a] , A. De Salvo[72a] , U. De Sanctis[73a,73b] ,
M. De Santis[73a,73b] , A. De Santo[155] , J.B. De Vivie De Regie[58] , D.V. Dedovich[79] , J. Degens[119] ,
A.M. Deiana[42] , J. Del Peso[98] , Y. Delabat Diaz[46] , F. Deliot[143] , C.M. Delitzsch[7] , M. Della Pietra[69a,69b] ,
D. Della Volpe[54] , A. Dell'Acqua[36] , L. Dell'Asta[68a,68b] , M. Delmastro[5] , C. Delporte[64] , P.A. Delsart[58] ,
S. Demers[181] , M. Demichev[79] , G. Demontigny[109] , S.P. Denisov[122] , L. D'Eramo[120] , D. Derendarz[84] ,
J.E. Derkaoui[35e] , F. Derue[134] , P. Dervan[90] , K. Desch[24] , K. Dette[165] , C. Deutsch[24] , P.O. Deviveiros[36] ,
F.A. Di Bello[72a,72b] , A. Di Ciaccio[73a,73b] , L. Di Ciaccio[5] , C. Di Donato[69a,69b] , A. Di Girolamo[36] ,
G. Di Gregorio[71a,71b] , A. Di Luca[75a,75b] , B. Di Micco[74a,74b] , R. Di Nardo[74a,74b] , C. Diaconu[101] ,
F.A. Dias[119] , T. Dias Do Vale[138a] , M.A. Diaz[145a] , F.G. Diaz Capriles[24] , J. Dickinson[18] , M. Didenko[164] ,
E.B. Diehl[105] , J. Dietrich[19] , S. Díez Cornell[46] , C. Diez Pardos[150] , A. Dimitrievska[18] , W. Ding[15b] ,
J. Dingfelder[24] , S.J. Dittmeier[61b] , F. Dittus[36] , F. Djama[101] , T. Djobava[158b] , J.I. Djuvsland[17] ,
M.A.B. Do Vale[146] , M. Dobre[27b] , D. Dodsworth[26] , C. Doglioni[96] , J. Dolejsi[141] , Z. Dolezal[141] ,
M. Donadelli[80c] , B. Dong[60c] , J. Donini[38] , A. D'onofrio[15c] , M. D'Onofrio[90] , J. Dopke[142] , A. Doria[69a] ,
M.T. Dova[88] , A.T. Doyle[57] , E. Drechsler[151] , E. Dreyer[151] , T. Dreyer[53] , A.S. Drobac[168] , D. Du[60b] ,
T.A. du Pree[119] , Y. Duan[60d] , F. Dubinin[110] , M. Dubovsky[28a] , A. Dubreuil[54] , E. Duchovni[178] ,
G. Duckeck[113] , O.A. Ducu[36,27b] , D. Duda[114] , A. Dudarev[36] , A.C. Dudder[99] , M. D'uffizi[100] , L. Duflot[64] ,
M. Dührssen[36] , C. Dülsen[180] , M. Dumancic[178] , A.E. Dumitriu[27b] , M. Dunford[61a] , S. Dungs[47] ,
A. Duperrin[101] , H. Duran Yildiz[4a] , M. Düren[56] , A. Durglishvili[158b] , B. Dutta[46] , D. Duvnjak[1] ,
G.I. Dyckes[135] , M. Dyndal[36] , S. Dysch[100] , B.S. Dziedzic[84] , B. Eckerova[28a] , M.G. Eggleston[49] ,
E. Egidio Purcino De Souza[80b] , L.F. Ehrke[54] , T. Eifert[8] , G. Eigen[17] , K. Einsweiler[18] , T. Ekelof[170] ,
V. Fabiani[118] , G. Facini[176] , R.M. Fakhrutdinov[122] , S. Falciano[72a] , P.J. Falke[24] , S. Falke[36] , J. Faltova[141] ,
H. El Jarrari[35f] , A. El Moussaouy[35a] , V. Ellajosyula[170] , M. Ellert[170] , F. Ellinghaus[180] , A.A. Elliot[92] ,
N. Ellis[36] , J. Elmsheuser[29] , M. Elsing[36] , D. Emeliyanov[142] , A. Emerman[39] , Y. Enari[162] , J. Erdmann[47] ,
A. Ereditato[20] , P.A. Erland[84] , M. Errenst[180] , M. Escalier[64] , C. Escobar[172] , O. Estrada Pastor[172] ,
E. Etzion[160] , G. Evans[138a] , H. Evans[65] , M.O. Evans[155] , A. Ezhilov[136] , F. Fabbri[57] , L. Fabbri[23b,23a] ,
Y. Fan[15a] , Y. Fang[15a] , Y. Fang[15a] , G. Fanourakis[44] , M. Fanti[68a,68b] , M. Faraj[60c] , A. Farbin[8] , A. Farilla[74a] ,
E.M. Farina[70a,70b] , T. Farooque[106] , S.M. Farrington[50] , P. Farthouat[36] , F. Fassi[35f] , D. Fassouliotis[9] ,
M. Faucci Giannelli[73a,73b] , W.J. Fawcett[32] , L. Fayard[64] , O.L. Fedin[136,p] , A. Fehr[20] , M. Feickert[171] ,
L. Feligioni[101] , A. Fell[148] , C. Feng[60b] , M. Feng[49] , M.J. Fenton[169] , A.B. Fenyuk[122] , S.W. Ferguson[43] ,
J. Ferrando[46] , A. Ferrari[170] , P. Ferrari[119] , R. Ferrari[70a] , D. Ferrere[54] , C. Ferretti[105] , F. Fiedler[99] ,
A. Filipčič[91] , F. Filthaut[118] , K.D. Finelli[25] , M.C.N. Fiolhais[138a,138c,a] , L. Fiorini[172] , F. Fischer[113] ,
J. Fischer[99] , W.C. Fisher[106] , T. Fitschen[21] , I. Fleck[150] , P. Fleischmann[105] , T. Flick[180] , B.M. Flierl[113] ,
L. Flores[135] , L.R. Flores Castillo[62a] , F.M. Follega[75a,75b] , N. Fomin[17] , J.H. Foo[165] , G.T. Forcolin[75a,75b] ,
B.C. Forland[65] , A. Formica[143] , F.A. Förster[14] , A.C. Forti[100] , E. Fortin[101] , M.G. Foti[133] , D. Fournier[64] ,
H. Fox[89] , P. Francavilla[71a,71b] , S. Francescato[72a,72b] , M. Franchini[23b,23a] , S. Franchino[61a] , D. Francis[36] ,
L. Franco[5] , L. Franconi[20] , M. Franklin[59] , G. Frattari[72a,72b] , P.M. Freeman[21] , B. Freund[109] ,
W.S. Freund[80b] , E.M. Freundlich[47] , D.C. Frizzell[127] , D. Froidevaux[36] , J.A. Frost[133] , Y. Fu[60a] ,
M. Fujimoto[125] , E. Fullana Torregrosa[172] , T. Fusayasu[115] , J. Fuster[172] , A. Gabrielli[23b,23a] , A. Gabrielli[36] ,
P. Gadow[114] , G. Gagliardi[55b,55a] , L.G. Gagnon[109] , G.E. Gallardo[133] , E.J. Gallas[133] , B.J. Gallop[142] ,
R. Gamboa Goni[92] , K.K. Gan[126] , S. Ganguly[178] , J. Gao[60a] , Y. Gao[50] , Y.S. Gao[31,m] , F.M. Garay Walls[145a] ,
C. García[172] , J.E. García Navarro[172] , J.A. García Pascual[15a] , M. Garcia-Sciveres[18] , R.W. Gardner[37] ,
S. Gargiulo[52] , C.A. Garner[165] , V. Garonne[132] , S.J. Gasiorowski[147] , P. Gaspar[80b] , G. Gaudio[70a] ,
P. Gauzzi[72a,72b] , I.L. Gavrilenko[110] , A. Gavrilyuk[123] , C. Gay[173] , G. Gaycken[46] , E.N. Gazis[10] ,
A.A. Geanta[27b] , C.M. Gee[144] , C.N.P. Gee[142] , J. Geisen[96] , M. Geisen[99] , C. Gemme[55b] , M.H. Genest[58] ,
C. Geng[105] , S. Gentile[72a,72b] , S. George[93] , T. Geralis[44] , L.O. Gerlach[53] , P. Gessinger-Befurt[99] ,
G. Gessner[47] , M. Ghasemi Bostanabad[174] , M. Ghneimat[150] , A. Ghosh[169] , A. Ghosh[77] , B. Giacobbe[23b] ,
S. Giagu[72a,72b] , N. Giangiacomi[165] , P. Giannetti[71a] , A. Giannini[69a,69b] , S.M. Gibson[93] , M. Gignac[144] ,
D.T. Gil[83b] , B.J. Gilbert[39] , D. Gillberg[34] , G. Gilles[180] , N.E.K. Gillwald[46] , D.M. Gingrich[3,ak] ,

M.P. Giordani[166a,66c], P.F. Giraud[143], G. Giugliarelli[166a,66c], D. Giugni[68a], F. Giuli[73a,73b], S. Gkaitatzis[161], I. Gkialas[9,h], E.L. Gkougkousis[14], P. Gkountoumis[10], L.K. Gladilin[112], C. Glasman[98], G.R. Gledhill[130], I. Gnesi[41b,c], M. Goblirsch-Kolb[26], D. Godin[109], S. Goldfarb[104], T. Golling[54], D. Golubkov[122], A. Gomes[138a,138b], R. Goncalves Gama[53], R. Gonçalo[138a,138c], G. Gonella[130], L. Gonella[21], A. Gongadze[79], F. Gonnella[21], J.L. Gonski[39], S. González de la Hoz[172], S. Gonzalez Fernandez[14], R. Gonzalez Lopez[90], C. Gonzalez Renteria[18], R. Gonzalez Suarez[170], S. Gonzalez-Sevilla[54], G.R. Gonzalvo Rodriguez[172], L. Goossens[36], N.A. Gorasia[21], P.A. Gorbounov[123], H.A. Gordon[29], B. Gorini[36], E. Gorini[67a,67b], A. Gorišek[91], A.T. Goshaw[49], M.I. Gostkin[79], C.A. Gottardo[118], M. Gouighri[35b], A.G. Goussiou[147], N. Govender[33c], C. Goy[5], I. Grabowska-Bold[83a], E. Gramstad[132], S. Grancagnolo[19], M. Grandi[155], V. Gratchev[136], P.M. Gravila[27f], F.G. Gravili[67a,67b], C. Gray[57], H.M. Gray[18], C. Grefe[24], I.M. Gregor[46], P. Grenier[152], K. Grevtsov[46], C. Grieco[14], N.A. Grieser[127], A.A. Grillo[144], K. Grimm[31,l], S. Grinstein[14,w], J.-F. Grivaz[64], S. Groh[99], E. Gross[178], J. Grosse-Knetter[53], Z.J. Grout[94], C. Grud[105], A. Grummer[117], J.C. Grundy[133], L. Guan[105], W. Guan[179], C. Gubbels[173], J. Guenther[36], J.G.R. Guerrero Rojas[172], F. Guescini[114], D. Guest[19], R. Gugel[99], A. Guida[46], T. Guillemin[5], S. Guindon[36], J. Guo[60c], L. Guo[64], Y. Guo[105], Z. Guo[101], R. Gupta[46], S. Gurbuz[24], G. Gustavino[127], M. Guth[52], P. Gutierrez[127], L.F. Gutierrez Zagazeta[135], C. Gutschow[94], C. Guyot[143], C. Gwenlan[133], C.B. Gwilliam[90], E.S. Haaland[132], A. Haas[124], M.H. Habedank[19], C. Haber[18], H.K. Hadavand[8], A. Hadef[99], M. Haleem[175], J. Haley[128], J.J. Hall[148], G. Halladjian[106], G.D. Hallewell[101], K. Hamano[174], H. Hamdaoui[35f], M. Hamer[24], G.N. Hamity[50], K. Han[60a], L. Han[15c], L. Han[60a], S. Han[18], Y.F. Han[165], K. Hanagaki[81,u], M. Hance[144], M.D. Hank[37], R. Hankache[100], E. Hansen[96], J.B. Hansen[40], J.D. Hansen[40], M.C. Hansen[24], P.H. Hansen[40], E.C. Hanson[100], K. Hara[167], T. Harenberg[180], S. Harkusha[107], P.F. Harrison[176], N.M. Hartman[152], N.M. Hartmann[113], Y. Hasegawa[149], A. Hasib[50], S. Hassani[143], S. Haug[20], R. Hauser[106], M. Havranek[140], C.M. Hawkes[21], R.J. Hawkings[36], S. Hayashida[116], D. Hayden[106], C. Hayes[105], R.L. Hayes[173], C.P. Hays[133], J.M. Hays[92], H.S. Hayward[90], S.J. Haywood[142], F. He[60a], Y. He[163], Y. He[134], M.P. Heath[50], V. Hedberg[96], A.L. Heggelund[132], N.D. Hehir[92], C. Heidegger[52], K.K. Heidegger[52], W.D. Heidorn[78], J. Heilman[34], S. Heim[46], T. Heim[18], B. Heinemann[46,ai], J.G. Heinlein[135], J.J. Heinrich[130], L. Heinrich[36], J. Hejbal[139], L. Helary[46], A. Held[124], S. Hellesund[132], C.M. Helling[144], S. Hellman[45a,45b], C. Helsens[36], R.C.W. Henderson[89], L. Henkelmann[32], A.M. Henriques Correia[36], H. Herde[152], Y. Hernández Jiménez[33f], H. Herr[99], M.G. Herrmann[113], T. Herrmann[48], G. Herten[52], R. Hertenberger[113], L. Hervas[36], N.P. Hessey[166a], H. Hibi[82], S. Higashino[81], E. Higón-Rodriguez[172], K. Hildebrand[37], K.K. Hill[29], K.H. Hiller[46], S.J. Hillier[21], M. Hils[48], I. Hinchliffe[18], F. Hinterkeuser[24], M. Hirose[131], S. Hirose[167], D. Hirschbuehl[180], B. Hiti[91], O. Hladik[139], J. Hobbs[154], R. Hobincu[27e], N. Hod[178], M.C. Hodgkinson[148], A. Hoecker[36], M.R. Hoeferkamp[117], D. Hohn[52], T. Holm[24], T.R. Holmes[37], M. Holzbock[114], L.B.A.H. Hommels[32], B.P. Honan[100], T.M. Hong[137], J.C. Honig[52], A. Hönle[114], B.H. Hooberman[171], W.H. Hopkins[6], Y. Horii[116], P. Horn[48], L.A. Horyn[37], S. Hou[157], J. Howarth[57], J. Hoya[88], M. Hrabovsky[129], A. Hrynevich[108], T. Hryn'ova[5], P.J. Hsu[63], S.-C. Hsu[147], Q. Hu[39], S. Hu[60c], Y.F. Hu[15a,15d,am], D.P. Huang[94], X. Huang[15c], Y. Huang[60a], Y. Huang[15a], Z. Hubacek[140], F. Hubaut[101], M. Huebner[24], F. Huegging[24], T.B. Huffman[133], M. Huhtinen[36], R. Hulsken[58], R.F.H. Hunter[34], N. Huseynov[79,ab], J. Huston[106], J. Huth[59], R. Hyneman[152], S. Hyrych[28a], G. Iacobucci[54], G. Iakovidis[29], I. Ibragimov[150], L. Iconomidou-Fayard[64], P. Iengo[36], R. Ignazzi[40], R. Iguchi[162], T. Iizawa[54], Y. Ikegami[81], N. Ilic[165,165], H. Imam[35a], G. Introzzi[70a,70b], M. Iodice[74a], K. Iordanidou[166a], V. Ippolito[72a,72b], M. Ishino[162], W. Islam[128], C. Issever[19,46], S. Istin[12c], J.M. Iturbe Ponce[62a], R. Iuppa[75a,75b], A. Ivina[178], J.M. Izen[43], V. Izzo[69a], P. Jacka[139], P. Jackson[1], R.M. Jacobs[46], B.P. Jaeger[151], C.S. Jagfeld[113], G. Jäkel[180], K.B. Jakobi[99], K. Jakobs[52], T. Jakoubek[178], J. Jamieson[57], K.W. Janas[83a], P.A. Janus[83a], G. Jarlskog[96], A.E. Jaspan[90], N. Javadov[79,ab], T. Javůrek[36], M. Javurkova[102], F. Jeanneau[143], L. Jeanty[130], J. Jejelava[158a], P. Jenni[52,d], S. Jézéquel[5], J. Jia[154], Z. Jia[15c], Y. Jiang[60a], S. Jiggins[52], F.A. Jimenez Morales[38], J. Jimenez Pena[114], S. Jin[15c], A. Jinaru[27b], O. Jinnouchi[163], H. Jivan[33f], P. Johansson[148], K.A. Johns[7],

C.A. Johnson[65], E. Jones[176], R.W.L. Jones[89], T.J. Jones[90], J. Jovicevic[36], X. Ju[18], J.J. Junggeburth[114],
A. Juste Rozas[14,w], A. Kaczmarska[84], M. Kado[72a,72b], H. Kagan[126], M. Kagan[152], A. Kahn[39], C. Kahra[99],
T. Kaji[177], E. Kajomovitz[159], C.W. Kalderon[29], A. Kaluza[99], A. Kamenshchikov[122], M. Kaneda[162],
N.J. Kang[144], S. Kang[78], Y. Kano[116], J. Kanzaki[81], D. Kar[33f], K. Karava[133], M.J. Kareem[166b],
I. Karkanias[161], S.N. Karpov[79], Z.M. Karpova[79], V. Kartvelishvili[89], A.N. Karyukhin[122], E. Kasimi[161],
C. Kato[60d], J. Katzy[46], K. Kawade[149], K. Kawagoe[87], T. Kawaguchi[116], T. Kawamoto[143], G. Kawamura[53],
E.F. Kay[174], F.I. Kaya[168], S. Kazakos[14], V.F. Kazanin[121b,121a], Y. Ke[154], J.M. Keaveney[33a], R. Keeler[174],
J.S. Keller[34], D. Kelsey[155], J.J. Kempster[21], J. Kendrick[21], K.E. Kennedy[39], O. Kepka[139], S. Kersten[180],
B.P. Kerševan[91], S. Ketabchi Haghighat[165], F. Khalil-Zada[13], M. Khandoga[143], A. Khanov[128],
A.G. Kharlamov[121b,121a], T. Kharlamova[121b,121a], E.E. Khoda[173], T.J. Khoo[19], G. Khoriauli[175],
E. Khramov[79], J. Khubua[158b], S. Kido[82], M. Kiehn[36], A. Kilgallon[130], E. Kim[163], Y.K. Kim[37],
N. Kimura[94], A. Kirchhoff[53], D. Kirchmeier[48], J. Kirk[142], A.E. Kiryunin[114], T. Kishimoto[162],
D.P. Kisliuk[165], V. Kitali[46], C. Kitsaki[10], O. Kivernyk[24], T. Klapdor-Kleingrothaus[52], M. Klassen[61a],
C. Klein[34], L. Klein[175], M.H. Klein[105], M. Klein[90], U. Klein[90], P. Klimek[36], A. Klimentov[29],
F. Klimpel[36], T. Klingl[24], T. Klioutchnikova[36], F.F. Klitzner[113], P. Kluit[119], S. Kluth[114], E. Kneringer[76],
A. Knue[52], D. Kobayashi[87], M. Kobel[48], M. Kocian[152], T. Kodama[162], P. Kodys[141], D.M. Koeck[155],
P.T. Koenig[24], T. Koffas[34], N.M. Köhler[36], M. Kolb[143], I. Koletsou[5], T. Komarek[129], K. Köneke[52],
A.X.Y. Kong[1], T. Kono[125], V. Konstantinides[94], N. Konstantinidis[94], B. Konya[96], R. Kopeliansky[65],
S. Koperny[83a], K. Korcyl[84], K. Kordas[161], G. Koren[160], A. Korn[94], S. Korn[53], I. Korolkov[14],
E.V. Korolkova[148], N. Korotkova[112], O. Kortner[114], S. Kortner[114], V.V. Kostyukhin[148,164],
A. Kotsokechagia[64], A. Kotwal[49], A. Koulouris[10], A. Kourkoumeli-Charalampidi[70a,70b],
C. Kourkoumelis[9], E. Kourlitis[6], R. Kowalewski[174], W. Kozanecki[143], A.S. Kozhin[122],
V.A. Kramarenko[112], G. Kramberger[91], D. Krasnopevtsev[60a], M.W. Krasny[134], A. Krasznahorkay[36],
J.A. Kremer[99], J. Kretzschmar[90], K. Kreul[19], P. Krieger[165], F. Krieter[113], S. Krishnamurthy[102],
A. Krishnan[61b], M. Krivos[141], K. Krizka[18], K. Kroeninger[47], H. Kroha[114], J. Kroll[139], J. Kroll[135],
K.S. Krowpman[106], U. Kruchonak[79], H. Krüger[24], N. Krumnack[78], M.C. Kruse[49], J.A. Krzysiak[84],
A. Kubota[163], O. Kuchinskaia[164], S. Kuday[4b], D. Kuechler[46], J.T. Kuechler[46], S. Kuehn[36], T. Kuhl[46],
V. Kukhtin[79], Y. Kulchitsky[107,ae], S. Kuleshov[145b], M. Kumar[33f], M. Kuna[58], A. Kupco[139], T. Kupfer[47],
O. Kuprash[52], H. Kurashige[82], L.L. Kurchaninov[166a], Y.A. Kurochkin[107], A. Kurova[111],
M.G. Kurth[15a,15d], E.S. Kuwertz[36], M. Kuze[163], A.K. Kvam[147], J. Kvita[129], T. Kwan[103], C. Lacasta[172],
F. Lacava[72a,72b], D.P.J. Lack[100], H. Lacker[19], D. Lacour[134], E. Ladygin[79], R. Lafaye[5], B. Laforge[134],
T. Lagouri[145c], S. Lai[53], I.K. Lakomiec[83a], J.E. Lambert[127], S. Lammers[65], W. Lampl[7], C. Lampoudis[161],
E. Lançon[29], U. Landgraf[52], M.P.J. Landon[92], V.S. Lang[52], J.C. Lange[53], R.J. Langenberg[102],
A.J. Lankford[169], F. Lanni[29], K. Lantzsch[24], A. Lanza[70a], A. Lapertosa[55b,55a], J.F. Laporte[143], T. Lari[68a],
F. Lasagni Manghi[23b,23a], M. Lassnig[36], V. Latonova[139], T.S. Lau[62a], A. Laudrain[99], A. Laurier[34],
M. Lavorgna[69a,69b], S.D. Lawlor[93], M. Lazzaroni[68a,68b], B. Le[100], A. Lebedev[78], M. LeBlanc[7],
T. LeCompte[6], F. Ledroit-Guillon[58], A.C.A. Lee[94], C.A. Lee[29], G.R. Lee[17], L. Lee[59], S.C. Lee[157],
S. Lee[78], L.L. Leeuw[33c], B. Lefebvre[166a], H.P. Lefebvre[93], M. Lefebvre[174], C. Leggett[18], K. Lehmann[151],
N. Lehmann[20], G. Lehmann Miotto[36], W.A. Leight[46], A. Leisos[161,v], M.A.L. Leite[80c], C.E. Leitgeb[113],
R. Leitner[141], K.J.C. Leney[42], T. Lenz[24], S. Leone[71a], C. Leonidopoulos[50], A. Leopold[134], C. Leroy[109],
R. Les[106], C.G. Lester[32], M. Levchenko[136], J. Levêque[5], D. Levin[105], L.J. Levinson[178], D.J. Lewis[21],
B. Li[15b], B. Li[105], C-Q. Li[60c,60d], F. Li[60c], H. Li[60a], H. Li[60b], J. Li[60c], K. Li[147], L. Li[60c], M. Li[15a,15d],
Q.Y. Li[60a], S. Li[60d,60c,b], X. Li[46], Y. Li[46], Z. Li[60b], Z. Li[133], Z. Li[103], Z. Li[90], Z. Liang[15a],
M. Liberatore[46], B. Liberti[73a], K. Lie[62c], C.Y. Lin[32], K. Lin[106], R.A. Linck[65], R.E. Lindley[7],
J.H. Lindon[21], A. Linss[46], A.L. Lionti[54], E. Lipeles[135], A. Lipniacka[17], T.M. Liss[171,aj], A. Lister[173],
J.D. Little[8], B. Liu[15a], B.X. Liu[151], J.B. Liu[60a], J.K.K. Liu[37], K. Liu[60d,60c], M. Liu[60a], M.Y. Liu[60a],
P. Liu[15a], X. Liu[60a], Y. Liu[46], Y. Liu[15a,15d], Y.L. Liu[105], Y.W. Liu[60a], M. Livan[70a,70b], A. Lleres[58],
J. Llorente Merino[151], S.L. Lloyd[92], E.M. Lobodzinska[46], P. Loch[7], S. Loffredo[73a,73b], T. Lohse[19],

K. Lohwasser[148], M. Lokajicek[139], J.D. Long[171], R.E. Long[89], I. Longarini[72a,72b], L. Longo[36], R. Longo[171], I. Lopez Paz[14], A. Lopez Solis[46], J. Lorenz[113], N. Lorenzo Martinez[5], A.M. Lory[113], A. Lösle[52], X. Lou[45a,45b], X. Lou[15a], A. Lounis[64], J. Love[6], P.A. Love[89], J.J. Lozano Bahilo[172], G. Lu[15a], M. Lu[60a], S. Lu[135], Y.J. Lu[63], H.J. Lubatti[147], C. Luci[72a,72b], F.L. Lucio Alves[15c], A. Lucotte[58], F. Luehring[65], I. Luise[154], L. Luminari[72a], B. Lund-Jensen[153], N.A. Luongo[130], M.S. Lutz[160], D. Lynn[29], H. Lyons[90], R. Lysak[139], E. Lytken[96], F. Lyu[15a], V. Lyubushkin[79], T. Lyubushkina[79], H. Ma[29], L.L. Ma[60b], Y. Ma[94], D.M. Mac Donell[174], G. Maccarrone[51], C.M. Macdonald[148], J.C. MacDonald[148], J. Machado Miguens[135], R. Madar[38], W.F. Mader[48], M. Madugoda Ralalage Don[128], N. Madysa[48], J. Maeda[82], T. Maeno[29], M. Maerker[48], V. Magerl[52], J. Magro[66a,66c], D.J. Mahon[39], C. Maidantchik[80b], A. Maio[138a,138b,138d], K. Maj[83a], O. Majersky[28a], S. Majewski[130], N. Makovec[64], B. Malaescu[134], Pa. Malecki[84], V.P. Maleev[136], F. Malek[58], D. Malito[41b,41a], U. Mallik[77], C. Malone[32], S. Maltezos[10], S. Malyukov[79], J. Mamuzic[172], G. Mancini[51], J.P. Mandalia[92], I. Mandić[91], L. Manhaes de Andrade Filho[80a], I.M. Maniatis[161], M. Manisha[143], J. Manjarres Ramos[48], K.H. Mankinen[96], A. Mann[113], A. Manousos[76], B. Mansoulie[143], I. Manthos[161], S. Manzoni[119], A. Marantis[161,v], L. Marchese[133], G. Marchiori[134], M. Marcisovsky[139], L. Marcoccia[73a,73b], C. Marcon[96], M. Marjanovic[127], Z. Marshall[18], M.U.F. Martensson[170], S. Marti-Garcia[172], T.A. Martin[176], V.J. Martin[50], B. Martin dit Latour[17], L. Martinelli[74a,74b], M. Martinez[14,w], P. Martinez Agullo[172], V.I. Martinez Outschoorn[102], S. Martin-Haugh[142], V.S. Martoiu[27b], A.C. Martyniuk[94], A. Marzin[36], S.R. Maschek[114], L. Masetti[99], T. Mashimo[162], R. Mashinistov[110], J. Masik[100], A.L. Maslennikov[121b,121a], L. Massa[23b,23a], P. Massarotti[69a,69b], P. Mastrandrea[71a,71b], A. Mastroberardino[41b,41a], T. Masubuchi[162], D. Matakias[29], T. Mathisen[170], A. Matic[113], N. Matsuzawa[162], J. Maurer[27b], B. Maček[91], D.A. Maximov[121b,121a], R. Mazini[157], I. Maznas[161], S.M. Mazza[144], C. Mc Ginn[29], J.P. Mc Gowan[103], S.P. Mc Kee[105], T.G. McCarthy[114], W.P. McCormack[18], E.F. McDonald[104], A.E. McDougall[119], J.A. Mcfayden[155], G. Mchedlidze[158b], M.A. McKay[42], K.D. McLean[174], S.J. McMahon[142], P.C. McNamara[104], R.A. McPherson[174,aa], J.E. Mdhluli[33f], Z.A. Meadows[102], S. Meehan[36], T. Megy[38], S. Mehlhase[113], A. Mehta[90], B. Meirose[43], D. Melini[159], B.R. Mellado Garcia[33f], F. Meloni[46], A. Melzer[24], E.D. Mendes Gouveia[138a,138e], A.M. Mendes Jacques Da Costa[21], H.Y. Meng[165], L. Meng[36], S. Menke[114], E. Meoni[41b,41a], S.A.M. Merkt[137], C. Merlassino[133], P. Mermod[54,*], L. Merola[69a,69b], C. Meroni[68a], G. Merz[105], O. Meshkov[112,110], J.K.R. Meshreki[150], J. Metcalfe[6], A.S. Mete[6], C. Meyer[65], J-P. Meyer[143], M. Michetti[19], R.P. Middleton[142], L. Mijović[50], G. Mikenberg[178], M. Mikestikova[139], M. Mikuž[91], H. Mildner[148], A. Milic[165], C.D. Milke[42], D.W. Miller[37], L.S. Miller[34], A. Milov[178], D.A. Milstead[45a,45b], A.A. Minaenko[122], I.A. Minashvili[158b], L. Mince[57], A.I. Mincer[124], B. Mindur[83a], M. Mineev[79], Y. Minegishi[162], Y. Mino[85], L.M. Mir[14], M. Miralles Lopez[172], M. Mironova[133], T. Mitani[177], V.A. Mitsou[172], M. Mittal[60c], O. Miu[165], A. Miucci[20], P.S. Miyagawa[92], A. Mizukami[81], J.U. Mjörnmark[96], T. Mkrtchyan[61a], M. Mlynarikova[120], T. Moa[45a,45b], S. Mobius[53], K. Mochizuki[109], P. Moder[46], P. Mogg[113], S. Mohapatra[39], G. Mokgatitswane[33f], B. Mondal[150], S. Mondal[140], K. Mönig[46], E. Monnier[101], A. Montalbano[151], J. Montejo Berlingen[36], M. Montella[94], F. Monticelli[88], N. Morange[64], A.L. Moreira De Carvalho[138a], M. Moreno Llácer[172], C. Moreno Martinez[14], P. Morettini[55b], M. Morgenstern[159], S. Morgenstern[176], D. Mori[151], M. Morii[59], M. Morinaga[177], V. Morisbak[132], A.K. Morley[36], A.P. Morris[94], L. Morvaj[36], P. Moschovakos[36], B. Moser[119], M. Mosidze[158b], T. Moskalets[143], P. Moskvitina[118], J. Moss[31,n], E.J.W. Moyse[102], S. Muanza[101], J. Mueller[137], D. Muenstermann[89], G.A. Mullier[96], J.J. Mullin[135], D.P. Mungo[68a,68b], J.L. Munoz Martinez[14], F.J. Munoz Sanchez[100], P. Murin[28b], W.J. Murray[176,142], A. Murrone[68a,68b], J.M. Muse[127], M. Muškinja[18], C. Mwewa[29], A.G. Myagkov[122,af], A.A. Myers[137], G. Myers[65], J. Myers[130], M. Myska[140], B.P. Nachman[18], O. Nackenhorst[47], A.Nag Nag[48], K. Nagai[133], K. Nagano[81], J.L. Nagle[29], E. Nagy[101], A.M. Nairz[36], Y. Nakahama[116], K. Nakamura[81], H. Nanjo[131], F. Napolitano[61a], R.F. Naranjo Garcia[46], R. Narayan[42], I. Naryshkin[136], M. Naseri[34], T. Naumann[46], G. Navarro[22a], J. Navarro-Gonzalez[172], P.Y. Nechaeva[110], F. Nechansky[46], T.J. Neep[21], A. Negri[70a,70b], M. Negrini[23b], C. Nellist[118], C. Nelson[103],

K. Nelson[105], M.E. Nelson[45a,45b], S. Nemecek[139], M. Nessi[36,f], M.S. Neubauer[171], F. Neuhaus[99],
M. Neumann[180], R. Newhouse[173], P.R. Newman[21], C.W. Ng[137], Y.S. Ng[19], Y.W.Y. Ng[169], B. Ngair[35f],
H.D.N. Nguyen[101], T. Nguyen Manh[109], E. Nibigira[38], R.B. Nickerson[133], R. Nicolaidou[143],
D.S. Nielsen[40], J. Nielsen[144], M. Niemeyer[53], N. Nikiforou[11], V. Nikolaenko[122,af], I. Nikolic-Audit[134],
K. Nikolopoulos[21], P. Nilsson[29], H.R. Nindhito[54], A. Nisati[72a], N. Nishu[60c], R. Nisius[114], T. Nitta[177],
T. Nobe[162], D.L. Noel[32], Y. Noguchi[85], I. Nomidis[134], M.A. Nomura[29], R.R.B. Norisam[94], J. Novak[91],
T. Novak[46], O. Novgorodova[48], R. Novotny[117], L. Nozka[129], K. Ntekas[169], E. Nurse[94], F.G. Oakham[34,ak],
J. Ocariz[134], A. Ochi[82], I. Ochoa[138a], J.P. Ochoa-Ricoux[145a], K. O'Connor[26], S. Oda[87], S. Odaka[81],
S. Oerdek[53], A. Ogrodnik[83a], A. Oh[100], C.C. Ohm[153], H. Oide[163], R. Oishi[162], M.L. Ojeda[165],
Y. Okazaki[85], M.W. O'Keefe[90], Y. Okumura[162], A. Olariu[27b], L.F. Oleiro Seabra[138a],
S.A. Olivares Pino[145c], D. Oliveira Damazio[29], D. Oliveira Goncalves[80a], J.L. Oliver[1], M.J.R. Olsson[169],
A. Olszewski[84], J. Olszowska[84], Ö.O. Öncel[24], D.C. O'Neil[151], A.P. O'neill[133], A. Onofre[138a,138e],
P.U.E. Onyisi[11], H. Oppen[132], R.G. Oreamuno Madriz[120], M.J. Oreglia[37], G.E. Orellana[88],
D. Orestano[74a,74b], N. Orlando[14], R.S. Orr[165], V. O'Shea[57], R. Ospanov[60a], G. Otero y Garzon[30],
H. Otono[87], P.S. Ott[61a], G.J. Ottino[18], M. Ouchrif[35e], J. Ouellette[29], F. Ould-Saada[132], A. Ouraou[143,*],
Q. Ouyang[15a], M. Owen[57], R.E. Owen[142], V.E. Ozcan[12c], N. Ozturk[8], J. Pacalt[129], H.A. Pacey[32],
K. Pachal[49], A. Pacheco Pages[14], C. Padilla Aranda[14], S. Pagan Griso[18], G. Palacino[65], S. Palazzo[50],
S. Palestini[36], M. Palka[83b], P. Palni[83a], D.K. Panchal[11], C.E. Pandini[54], J.G. Panduro Vazquez[93], P. Pani[46],
G. Panizzo[66a,66c], L. Paolozzi[54], C. Papadatos[109], S. Parajuli[42], A. Paramonov[6], C. Paraskevopoulos[10],
D. Paredes Hernandez[62b], S.R. Paredes Saenz[133], B. Parida[178], T.H. Park[165], A.J. Parker[31], M.A. Parker[32],
F. Parodi[55b,55a], E.W. Parrish[120], J.A. Parsons[39], U. Parzefall[52], L. Pascual Dominguez[134], V.R. Pascuzzi[18],
J.M.P. Pasner[144], F. Pasquali[119], E. Pasqualucci[72a], S. Passaggio[55b], F. Pastore[93], P. Pasuwan[45a,45b],
J.R. Pater[100], A. Pathak[179,j], J. Patton[90], T. Pauly[36], J. Pearkes[152], M. Pedersen[132], L. Pedraza Diaz[118],
R. Pedro[138a], T. Peiffer[53], S.V. Peleganchuk[121b,121a], O. Penc[139], C. Peng[62b], H. Peng[60a], M. Penzin[164],
B.S. Peralva[80a], M.M. Perego[64], A.P. Pereira Peixoto[138a], L. Pereira Sanchez[45a,45b], D.V. Perepelitsa[29],
E. Perez Codina[166a], M. Perganti[10], L. Perini[68a,68b], H. Pernegger[36], S. Perrella[36], A. Perrevoort[119],
K. Peters[46], R.F.Y. Peters[100], B.A. Petersen[36], T.C. Petersen[40], E. Petit[101], V. Petousis[140], C. Petridou[161],
P. Petroff[64], F. Petrucci[74a,74b], M. Pettee[181], N.E. Pettersson[102], K. Petukhova[141], A. Peyaud[143],
R. Pezoa[145d], L. Pezzotti[70a,70b], G. Pezzullo[181], T. Pham[104], P.W. Phillips[142], M.W. Phipps[171],
G. Piacquadio[154], E. Pianori[18], A. Picazio[102], R. Piegaia[30], D. Pietreanu[27b], J.E. Pilcher[37],
A.D. Pilkington[100], M. Pinamonti[66a,66c], J.L. Pinfold[3], C. Pitman Donaldson[94], D.A. Pizzi[34],
L. Pizzimento[73a,73b], A. Pizzini[119], M.-A. Pleier[29], V. Plesanovs[52], V. Pleskot[141], E. Plotnikova[79],
P. Podberezko[121b,121a], R. Poettgen[96], R. Poggi[54], L. Poggioli[134], I. Pogrebnyak[106], D. Pohl[24],
I. Pokharel[53], G. Polesello[70a], A. Poley[151,166a], A. Policicchio[72a,72b], R. Polifka[141], A. Polini[23b],
C.S. Pollard[46], V. Polychronakos[29], D. Ponomarenko[111], L. Pontecorvo[36], S. Popa[27a], G.A. Popeneciu[27d],
L. Portales[5], D.M. Portillo Quintero[58], S. Pospisil[140], P. Postolache[27c], K. Potamianos[133], I.N. Potrap[79],
C.J. Potter[32], H. Potti[11], T. Poulsen[46], J. Poveda[172], T.D. Powell[148], G. Pownall[46],
M.E. Pozo Astigarraga[36], A. Prades Ibanez[172], P. Pralavorio[101], M.M. Prapa[44], S. Prell[78], D. Price[100],
M. Primavera[67a], M.L. Proffitt[147], N. Proklova[111], K. Prokofiev[62c], F. Prokoshin[79], S. Protopopescu[29],
J. Proudfoot[6], M. Przybycien[83a], D. Pudzha[136], P. Puzo[64], D. Pyatiizbyantseva[111], J. Qian[105], Y. Qin[100],
A. Quadt[53], M. Queitsch-Maitland[36], G. Rabanal Bolanos[59], F. Ragusa[68a,68b], G. Rahal[97], J.A. Raine[54],
S. Rajagopalan[29], K. Ran[15a,15d], D.F. Rassloff[61a], D.M. Rauch[46], S. Rave[99], B. Ravina[57], I. Ravinovich[178],
M. Raymond[36], A.L. Read[132], N.P. Readioff[148], M. Reale[67a,67b], D.M. Rebuzzi[70a,70b], G. Redlinger[29],
K. Reeves[43], D. Reikher[160], A. Reiss[99], A. Rej[150], C. Rembser[36], A. Renardi[46], M. Renda[27b],
M.B. Rendel[114], A.G. Rennie[57], S. Resconi[68a], E.D. Resseguie[18], S. Rettie[94], B. Reynolds[126],
E. Reynolds[21], M. Rezaei Estabragh[180], O.L. Rezanova[121b,121a], P. Reznicek[141], E. Ricci[75a,75b],
R. Richter[114], S. Richter[46], E. Richter-Was[83b], M. Ridel[134], P. Rieck[114], O. Rifki[46], M. Rijssenbeek[154],
A. Rimoldi[70a,70b], M. Rimoldi[46], L. Rinaldi[23b], T.T. Rinn[171], M.P. Rinnagel[113], G. Ripellino[153], I. Riu[14],

P. Rivadeneira[46], J.C. Rivera Vergara[174], F. Rizatdinova[128], E. Rizvi[92], C. Rizzi[54], S.H. Robertson[103,aa],
M. Robin[46], D. Robinson[32], C.M. Robles Gajardo[145d], M. Robles Manzano[99], A. Robson[57],
A. Rocchi[73a,73b], C. Roda[71a,71b], S. Rodriguez Bosca[172], A. Rodriguez Rodriguez[52],
A.M. Rodríguez Vera[166b], S. Roe[36], J. Roggel[180], O. Røhne[132], R.A. Rojas[145d], B. Roland[52],
C.P.A. Roland[65], J. Roloff[29], A. Romaniouk[111], M. Romano[23b,23a], N. Rompotis[90], M. Ronzani[124],
L. Roos[134], S. Rosati[72a], G. Rosin[102], B.J. Rosser[135], E. Rossi[165], E. Rossi[5], E. Rossi[69a,69b], L.P. Rossi[55b],
L. Rossini[46], R. Rosten[126], M. Rotaru[27b], B. Rottler[52], D. Rousseau[64], D. Rousso[32], G. Rovelli[70a,70b],
A. Roy[11], A. Rozanov[101], Y. Rozen[159], X. Ruan[33f], A.J. Ruby[90], T.A. Ruggeri[1], F. Rühr[52],
A. Ruiz-Martinez[172], A. Rummler[36], Z. Rurikova[52], N.A. Rusakovich[79], H.L. Russell[36], L. Rustige[38],
J.P. Rutherfoord[7], E.M. Rüttinger[148], M. Rybar[141], E.B. Rye[132], A. Ryzhov[122], J.A. Sabater Iglesias[46],
P. Sabatini[172], L. Sabetta[72a,72b], H.F-W. Sadrozinski[144], R. Sadykov[79], F. Safai Tehrani[72a],
B. Safarzadeh Samani[155], M. Safdari[152], P. Saha[120], S. Saha[103], M. Sahinsoy[114], A. Sahu[180],
M. Saimpert[36], M. Saito[162], T. Saito[162], D. Salamani[54], G. Salamanna[74a,74b], A. Salnikov[152], J. Salt[172],
A. Salvador Salas[14], D. Salvatore[41b,41a], F. Salvatore[155], A. Salzburger[36], D. Sammel[52],
D. Sampsonidis[161], D. Sampsonidou[60d,60c], J. Sánchez[172], A. Sanchez Pineda[66a,36,66c], H. Sandaker[132],
C.O. Sander[46], I.G. Sanderswood[89], M. Sandhoff[180], C. Sandoval[22b], D.P.C. Sankey[142], M. Sannino[55b,55a],
Y. Sano[116], A. Sansoni[51], C. Santoni[38], H. Santos[138a,138b], S.N. Santpur[18], A. Santra[178], K.A. Saoucha[148],
A. Sapronov[79], J.G. Saraiva[138a,138d], O. Sasaki[81], K. Sato[167], F. Sauerburger[52], E. Sauvan[5],
P. Savard[165,ak], R. Sawada[162], C. Sawyer[142], L. Sawyer[95], I. Sayago Galvan[172], C. Sbarra[23b],
A. Sbrizzi[66a,66c], T. Scanlon[94], J. Schaarschmidt[147], P. Schacht[114], D. Schaefer[37], L. Schaefer[135],
U. Schäfer[99], A.C. Schaffer[64], D. Schaile[113], R.D. Schamberger[154], E. Schanet[113], C. Scharf[19],
N. Scharmberg[100], V.A. Schegelsky[136], D. Scheirich[141], F. Schenck[19], M. Schernau[169], C. Schiavi[55b,55a],
L.K. Schildgen[24], Z.M. Schillaci[26], E.J. Schioppa[67a,67b], M. Schioppa[41b,41a], K.E. Schleicher[52],
S. Schlenker[36], K. Schmieden[99], C. Schmitt[99], S. Schmitt[46], L. Schoeffel[143], A. Schoening[61b],
P.G. Scholer[52], E. Schopf[133], M. Schott[99], J. Schovancova[36], S. Schramm[54], F. Schroeder[180], A. Schulte[99],
H-C. Schultz-Coulon[61a], M. Schumacher[52], B.A. Schumm[144], Ph. Schune[143], A. Schwartzman[152],
T.A. Schwarz[105], Ph. Schwemling[143], R. Schwienhorst[106], A. Sciandra[144], G. Sciolla[26], F. Scuri[71a],
F. Scutti[104], C.D. Sebastiani[90], K. Sedlaczek[47], P. Seema[19], S.C. Seidel[117], A. Seiden[144], B.D. Seidlitz[29],
T. Seiss[37], C. Seitz[46], J.M. Seixas[80b], G. Sekhniaidze[69a], S.J. Sekula[42], L.P. Selem[5],
N. Semprini-Cesari[23b,23a], S. Sen[49], C. Serfon[29], L. Serin[64], L. Serkin[66a,66b], M. Sessa[60a], H. Severini[127],
S. Sevova[152], F. Sforza[55b,55a], A. Sfyrla[54], E. Shabalina[53], J.D. Shahinian[135], N.W. Shaikh[45a,45b],
D. Shaked Renous[178], L.Y. Shan[15a], M. Shapiro[18], A. Sharma[36], A.S. Sharma[1], P.B. Shatalov[123],
K. Shaw[155], S.M. Shaw[100], M. Shehade[178], Y. Shen[127], P. Sherwood[94], L. Shi[94], C.O. Shimmin[181],
Y. Shimogama[177], M. Shimojima[115], J.D. Shinner[93], I.P.J. Shipsey[133], S. Shirabe[163], M. Shiyakova[79,y],
J. Shlomi[178], M.J. Shochet[37], J. Shojaii[104], D.R. Shope[153], S. Shrestha[126], E.M. Shrif[33f], M.J. Shroff[174],
E. Shulga[178], P. Sicho[139], A.M. Sickles[171], E. Sideras Haddad[33f], O. Sidiropoulou[36], A. Sidoti[23b,23a],
F. Siegert[48], Dj. Sijacki[16], M.V. Silva Oliveira[36], S.B. Silverstein[45a], S. Simion[64], R. Simoniello[36],
S. Simsek[12b], P. Sinervo[165], V. Sinetckii[112], S. Singh[151], S. Sinha[33f], M. Sioli[23b,23a], I. Siral[130],
S.Yu. Sivoklokov[112], J. Sjölin[45a,45b], A. Skaf[53], E. Skorda[96], P. Skubic[127], M. Slawinska[84], K. Sliwa[168],
V. Smakhtin[178], B.H. Smart[142], J. Smiesko[141], S.Yu. Smirnov[111], Y. Smirnov[111], L.N. Smirnova[112,r],
O. Smirnova[96], E.A. Smith[37], H.A. Smith[37], M. Smizanska[89], K. Smolek[140], A. Smykiewicz[84],
A.A. Snesarev[110], H.L. Snoek[119], I.M. Snyder[130], S. Snyder[29], R. Sobie[174,aa], A. Soffer[160], A. Søgaard[50],
F. Sohns[53], C.A. Solans Sanchez[36], E.Yu. Soldatov[111], U. Soldevila[172], A.A. Solodkov[122], S. Solomon[52],
A. Soloshenko[79], O.V. Solovyanov[122], V. Solovyev[136], P. Sommer[148], H. Son[168], A. Sonay[14],
W.Y. Song[166b], A. Sopczak[140], A.L. Sopio[94], F. Sopkova[28b], S. Sottocornola[70a,70b], R. Soualah[66a,66c],
A.M. Soukharev[121b,121a], Z. Soumaimi[35f], D. South[46], S. Spagnolo[67a,67b], M. Spalla[114],
M. Spangenberg[176], F. Spanò[93], D. Sperlich[52], T.M. Spieker[61a], G. Spigo[36], M. Spina[155], D.P. Spiteri[57],
M. Spousta[141], A. Stabile[68a,68b], B.L. Stamas[120], R. Stamen[61a], M. Stamenkovic[119], A. Stampekis[21],

E. Stanecka[84], B. Stanislaus[133], M.M. Stanitzki[46], M. Stankaityte[133], B. Stapf[119], E.A. Starchenko[122], G.H. Stark[144], J. Stark[101], D.M. Starko[166b], P. Staroba[139], P. Starovoitov[61a], S. Stärz[103], R. Staszewski[84], G. Stavropoulos[44], P. Steinberg[29], A.L. Steinhebel[130], B. Stelzer[151,166a], H.J. Stelzer[137], O. Stelzer-Chilton[166a], H. Stenzel[56], T.J. Stevenson[155], G.A. Stewart[36], M.C. Stockton[36], G. Stoicea[27b], M. Stolarski[138a], S. Stonjek[114], A. Straessner[48], J. Strandberg[153], S. Strandberg[45a,45b], M. Strauss[127], T. Strebler[101], P. Strizenec[28b], R. Ströhmer[175], D.M. Strom[130], L.R. Strom[46], R. Stroynowski[42], A. Strubig[45a,45b], S.A. Stucci[29], B. Stugu[17], J. Stupak[127], N.A. Styles[46], D. Su[152], W. Su[60d,147,60c], X. Su[60a], N.B. Suarez[137], K. Sugizaki[162], V.V. Sulin[110], M.J. Sullivan[90], D.M.S. Sultan[54], S. Sultansoy[4c], T. Sumida[85], S. Sun[105], S. Sun[179], X. Sun[100], C.J.E. Suster[156], M.R. Sutton[155], M. Svatos[139], M. Swiatlowski[166a], S.P. Swift[2], T. Swirski[175], A. Sydorenko[99], I. Sykora[28a], M. Sykora[141], T. Sykora[141], D. Ta[99], K. Tackmann[46,x], A. Taffard[169], R. Tafirout[166a], E. Tagiev[122], R.H.M. Taibah[134], R. Takashima[86], K. Takeda[82], T. Takeshita[149], E.P. Takeva[50], Y. Takubo[81], M. Talby[101], A.A. Talyshev[121b,121a], K.C. Tam[62b], N.M. Tamir[160], J. Tanaka[162], R. Tanaka[64], S. Tapia Araya[171], S. Tapprogge[99], A. Tarek Abouelfadl Mohamed[106], S. Tarem[159], K. Tariq[60b], G. Tarna[27b,e], G.F. Tartarelli[68a], P. Tas[141], M. Tasevsky[139], E. Tassi[41b,41a], G. Tateno[162], Y. Tayalati[35f], G.N. Taylor[104], W. Taylor[166b], H. Teagle[90], A.S. Tee[89], R. Teixeira De Lima[152], P. Teixeira-Dias[93], H. Ten Kate[36], J.J. Teoh[119], K. Terashi[162], J. Terron[98], S. Terzo[14], M. Testa[51], R.J. Teuscher[165,aa], N. Themistokleous[50], T. Theveneaux-Pelzer[19], D.W. Thomas[93], J.P. Thomas[21], E.A. Thompson[46], P.D. Thompson[21], E. Thomson[135], E.J. Thorpe[92], V.O. Tikhomirov[110,ag], Yu.A. Tikhonov[121b,121a], S. Timoshenko[111], P. Tipton[181], S. Tisserant[101], S.H. Tlou[33f], A. Tnourji[38], K. Todome[23b,23a], S. Todorova-Nova[141], S. Todt[48], M. Togawa[81], J. Tojo[87], S. Tokár[28a], K. Tokushuku[81], E. Tolley[126], R. Tombs[32], M. Tomoto[81,116], L. Tompkins[152], P. Tornambe[102], E. Torrence[130], H. Torres[48], E. Torró Pastor[172], M. Toscani[30], C. Tosciri[37], J. Toth[101,z], D.R. Tovey[148], A. Traet[17], C.J. Treado[124], T. Trefzger[175], A. Tricoli[29], I.M. Trigger[166a], S. Trincaz-Duvoid[134], D.A. Trischuk[173], W. Trischuk[165], B. Trocmé[58], A. Trofymov[64], C. Troncon[68a], F. Trovato[155], L. Truong[33c], M. Trzebinski[84], A. Trzupek[84], F. Tsai[46], P.V. Tsiareshka[107,ae], A. Tsirigotis[161,v], V. Tsiskaridze[154], E.G. Tskhadadze[158a], M. Tsopoulou[161], I.I. Tsukerman[123], V. Tsulaia[18], S. Tsuno[81], O. Tsur[159], D. Tsybychev[154], Y. Tu[62b], A. Tudorache[27b], V. Tudorache[27b], A.N. Tuna[36], S. Turchikhin[79], D. Turgeman[178], I. Turk Cakir[4b,t], R.J. Turner[21], R. Turra[68a], P.M. Tuts[39], S. Tzamarias[161], P. Tzanis[10], E. Tzovara[99], K. Uchida[162], F. Ukegawa[167], G. Unal[36], M. Unal[11], A. Undrus[29], G. Unel[169], F.C. Ungaro[104], K. Uno[162], J. Urban[28b], P. Urquijo[104], G. Usai[8], R. Ushioda[163], Z. Uysal[12d], V. Vacek[140], B. Vachon[103], K.O.H. Vadla[132], T. Vafeiadis[36], C. Valderanis[113], E. Valdes Santurio[45a,45b], M. Valente[166a], S. Valentinetti[23b,23a], A. Valero[172], L. Valéry[46], R.A. Vallance[21], A. Vallier[36], J.A. Valls Ferrer[172], T.R. Van Daalen[14], P. Van Gemmeren[6], S. Van Stroud[94], I. Van Vulpen[119], M. Vanadia[73a,73b], W. Vandelli[36], M. Vandenbroucke[143], E.R. Vandewall[128], D. Vannicola[72a,72b], R. Vari[72a], E.W. Varnes[7], C. Varni[55b,55a], T. Varol[157], D. Varouchas[64], K.E. Varvell[156], M.E. Vasile[27b], L. Vaslin[38], G.A. Vasquez[174], F. Vazeille[38], D. Vazquez Furelos[14], T. Vazquez Schroeder[36], J. Veatch[53], V. Vecchio[100], M.J. Veen[119], L.M. Veloce[165], F. Veloso[138a,138c], S. Veneziano[72a], A. Ventura[67a,67b], A. Verbytskyi[114], M. Verducci[71a,71b], C. Vergis[24], M. Verissimo De Araujo[80b], W. Verkerke[119], A.T. Vermeulen[119], J.C. Vermeulen[119], C. Vernieri[152], P.J. Verschuuren[93], M.L. Vesterbacka[124], M.C. Vetterli[151,ak], N. Viaux Maira[145d], T. Vickey[148], O.E. Vickey Boeriu[148], G.H.A. Viehhauser[133], L. Vigani[61b], M. Villa[23b,23a], M. Villaplana Perez[172], E.M. Villhauer[50], E. Vilucchi[51], M.G. Vincter[34], G.S. Virdee[21], A. Vishwakarma[50], C. Vittori[23b,23a], I. Vivarelli[155], V. Vladimirov[176], M. Vogel[180], P. Vokac[140], J. Von Ahnen[46], S.E. von Buddenbrock[33f], E. Von Toerne[24], V. Vorobel[141], K. Vorobev[111], M. Vos[172], J.H. Vossebeld[90], M. Vozak[100], N. Vranjes[16], M. Vranjes Milosavljevic[16], V. Vrba[140,*], M. Vreeswijk[119], N.K. Vu[101], R. Vuillermet[36], I. Vukotic[37], S. Wada[167], C. Wagner[102], P. Wagner[24], W. Wagner[180], S. Wahdan[180], H. Wahlberg[88], R. Wakasa[167], V.M. Walbrecht[114], J. Walder[142], R. Walker[113], S.D. Walker[93], W. Walkowiak[150], V. Wallangen[45a,45b], A.M. Wang[59], A.Z. Wang[179], C. Wang[60a], C. Wang[60c], H. Wang[18], J. Wang[62a], P. Wang[42], R.-J. Wang[99], R. Wang[99], R. Wang[60a], R. Wang[120], S.M. Wang[157],

S. Wang[60b], T. Wang[60a], W.T. Wang[60a], W.X. Wang[60a], X. Wang[171], Y. Wang[60a], Z. Wang[105], C. Wanotayaroj[36], A. Warburton[103], C.P. Ward[32], R.J. Ward[21], N. Warrack[57], A.T. Watson[21], M.F. Watson[21], G. Watts[147], B.M. Waugh[94], A.F. Webb[11], C. Weber[29], M.S. Weber[20], S.A. Weber[34], S.M. Weber[61a], C. Wei[60a], Y. Wei[133], A.R. Weidberg[133], J. Weingarten[47], M. Weirich[99], C. Weiser[52], P.S. Wells[36], T. Wenaus[29], B. Wendland[47], T. Wengler[36], S. Wenig[36], N. Wermes[24], M. Wessels[61a], T.D. Weston[20], K. Whalen[130], A.M. Wharton[89], A.S. White[59], A. White[8], M.J. White[1], D. Whiteson[169], W. Wiedenmann[179], C. Wiel[48], M. Wielers[142], N. Wieseotte[99], C. Wiglesworth[40], L.A.M. Wiik-Fuchs[52], H.G. Wilkens[36], L.J. Wilkins[93], D.M. Williams[39], H.H. Williams[135], S. Williams[32], S. Willocq[102], P.J. Windischhofer[133], I. Wingerter-Seez[5], F. Winklmeier[130], B.T. Winter[52], M. Wittgen[152], M. Wobisch[95], A. Wolf[99], R. Wölker[133], J. Wollrath[52], M.W. Wolter[84], H. Wolters[138a,138c], V.W.S. Wong[173], A.F. Wongel[46], N.L. Woods[144], S.D. Worm[46], B.K. Wosiek[84], K.W. Woźniak[84], K. Wraight[57], J. Wu[15a,15d], S.L. Wu[179], X. Wu[54], Y. Wu[60a], Z. Wu[143], J. Wuerzinger[133], T.R. Wyatt[100], B.M. Wynne[50], S. Xella[40], J. Xiang[62c], X. Xiao[105], X. Xie[60a], I. Xiotidis[155], D. Xu[15a], H. Xu[60a], H. Xu[60a], L. Xu[60a], R. Xu[135], T. Xu[143], W. Xu[105], Y. Xu[15b], Z. Xu[60b], Z. Xu[152], B. Yabsley[156], S. Yacoob[33a], D.P. Yallup[94], N. Yamaguchi[87], Y. Yamaguchi[163], M. Yamatani[162], H. Yamauchi[167], T. Yamazaki[18], Y. Yamazaki[82], J. Yan[60c], Z. Yan[25], H.J. Yang[60c,60d], H.T. Yang[18], S. Yang[60a], T. Yang[62c], X. Yang[60a], X. Yang[15a], Y. Yang[162], Z. Yang[105,60a], W-M. Yao[18], Y.C. Yap[46], H. Ye[15c], J. Ye[42], S. Ye[29], I. Yeletskikh[79], M.R. Yexley[89], P. Yin[39], K. Yorita[177], K. Yoshihara[78], C.J.S. Young[36], C. Young[152], R. Yuan[60b,i], X. Yue[61a], M. Zaazoua[35f], B. Zabinski[84], G. Zacharis[10], E. Zaffaroni[54], J. Zahreddine[101], A.M. Zaitsev[122,af], T. Zakareishvili[158b], N. Zakharchuk[34], S. Zambito[36], D. Zanzi[52], S.V. Zeißner[47], C. Zeitnitz[180], G. Zemaityte[133], J.C. Zeng[171], O. Zenin[122], T. Ženiš[28a], S. Zenz[92], S. Zerradi[35a], D. Zerwas[64], M. Zgubič[133], B. Zhang[15c], D.F. Zhang[15b], G. Zhang[15b], J. Zhang[6], K. Zhang[15a], L. Zhang[15c], L. Zhang[60a], M. Zhang[171], R. Zhang[179], S. Zhang[105], X. Zhang[60c], X. Zhang[60b], Z. Zhang[64], P. Zhao[49], Y. Zhao[144], Z. Zhao[60a], A. Zhemchugov[79], Z. Zheng[105], D. Zhong[171], B. Zhou[105], C. Zhou[179], H. Zhou[7], M. Zhou[154], N. Zhou[60c], Y. Zhou[7], C.G. Zhu[60b], C. Zhu[15a,15d], H.L. Zhu[60a], H. Zhu[15a], J. Zhu[105], Y. Zhu[60a], X. Zhuang[15a], K. Zhukov[110], V. Zhulanov[121b,121a], D. Zieminska[65], N.I. Zimine[79], S. Zimmermann[52,*], Z. Zinonos[114], M. Ziolkowski[150], L. Živković[16], A. Zoccoli[23b,23a], K. Zoch[53], T.G. Zorbas[148], R. Zou[37], W. Zou[39], L. Zwalinski[36].

1 Department of Physics, University of Adelaide, Adelaide; Australia
2 Physics Department, SUNY Albany, Albany NY; United States of America
3 Department of Physics, University of Alberta, Edmonton AB; Canada
4 (a) Department of Physics, Ankara University, Ankara; (b) Istanbul Aydin University, Application and Research Center for Advanced Studies, Istanbul; (c) Division of Physics, TOBB University of Economics and Technology, Ankara; Turkey
5 LAPP, Univ. Savoie Mont Blanc, CNRS/IN2P3, Annecy; France
6 High Energy Physics Division, Argonne National Laboratory, Argonne IL; United States of America
7 Department of Physics, University of Arizona, Tucson AZ; United States of America
8 Department of Physics, University of Texas at Arlington, Arlington TX; United States of America
9 Physics Department, National and Kapodistrian University of Athens, Athens; Greece
10 Physics Department, National Technical University of Athens, Zografou; Greece
11 Department of Physics, University of Texas at Austin, Austin TX; United States of America
12 (a) Bahcesehir University, Faculty of Engineering and Natural Sciences, Istanbul; (b) Istanbul Bilgi University, Faculty of Engineering and Natural Sciences, Istanbul; (c) Department of Physics, Bogazici University, Istanbul; (d) Department of Physics Engineering, Gaziantep University, Gaziantep; Turkey
13 Institute of Physics, Azerbaijan Academy of Sciences, Baku; Azerbaijan
14 Institut de Física d'Altes Energies (IFAE), Barcelona Institute of Science and Technology, Barcelona; Spain
15 (a) Institute of High Energy Physics, Chinese Academy of Sciences, Beijing; (b) Physics Department, Tsinghua University, Beijing; (c) Department of Physics, Nanjing University, Nanjing; (d) University of Chinese Academy of Science (UCAS), Beijing; China

16 Institute of Physics, University of Belgrade, Belgrade; Serbia

17 Department for Physics and Technology, University of Bergen, Bergen; Norway

18 Physics Division, Lawrence Berkeley National Laboratory and University of California, Berkeley CA; United States of America

19 Institut für Physik, Humboldt Universität zu Berlin, Berlin; Germany

20 Albert Einstein Center for Fundamental Physics and Laboratory for High Energy Physics, University of Bern, Bern; Switzerland

21 School of Physics and Astronomy, University of Birmingham, Birmingham; United Kingdom

22 (a)Facultad de Ciencias y Centro de Investigaciónes, Universidad Antonio Nariño, Bogotá; (b)Departamento de Física, Universidad Nacional de Colombia, Bogotá, Colombia; Colombia

23 (a)INFN Bologna and Universita' di Bologna, Dipartimento di Fisica; (b)INFN Sezione di Bologna; Italy

24 Physikalisches Institut, Universität Bonn, Bonn; Germany

25 Department of Physics, Boston University, Boston MA; United States of America

26 Department of Physics, Brandeis University, Waltham MA; United States of America

27 (a)Transilvania University of Brasov, Brasov; (b)Horia Hulubei National Institute of Physics and Nuclear Engineering, Bucharest; (c)Department of Physics, Alexandru Ioan Cuza University of Iasi, Iasi; (d)National Institute for Research and Development of Isotopic and Molecular Technologies, Physics Department, Cluj-Napoca; (e)University Politehnica Bucharest, Bucharest; (f)West University in Timisoara, Timisoara; Romania

28 (a)Faculty of Mathematics, Physics and Informatics, Comenius University, Bratislava; (b)Department of Subnuclear Physics, Institute of Experimental Physics of the Slovak Academy of Sciences, Kosice; Slovak Republic

29 Physics Department, Brookhaven National Laboratory, Upton NY; United States of America

30 Departamento de Física, Universidad de Buenos Aires, Buenos Aires; Argentina

31 California State University, CA; United States of America

32 Cavendish Laboratory, University of Cambridge, Cambridge; United Kingdom

33 (a)Department of Physics, University of Cape Town, Cape Town; (b)iThemba Labs, Western Cape; (c)Department of Mechanical Engineering Science, University of Johannesburg, Johannesburg; (d)National Institute of Physics, University of the Philippines Diliman; (e)University of South Africa, Department of Physics, Pretoria; (f)School of Physics, University of the Witwatersrand, Johannesburg; South Africa

34 Department of Physics, Carleton University, Ottawa ON; Canada

35 (a)Faculté des Sciences Ain Chock, Réseau Universitaire de Physique des Hautes Energies - Université Hassan II, Casablanca; (b)Faculté des Sciences, Université Ibn-Tofail, Kénitra; (c)Faculté des Sciences Semlalia, Université Cadi Ayyad, LPHEA-Marrakech; (d)Moroccan Foundation for Advanced Science Innovation and Research (MAScIR), Rabat; (e)LPMR, Faculté des Sciences, Université Mohamed Premier, Oujda; (f)Faculté des sciences, Université Mohammed V, Rabat; Morocco

36 CERN, Geneva; Switzerland

37 Enrico Fermi Institute, University of Chicago, Chicago IL; United States of America

38 LPC, Université Clermont Auvergne, CNRS/IN2P3, Clermont-Ferrand; France

39 Nevis Laboratory, Columbia University, Irvington NY; United States of America

40 Niels Bohr Institute, University of Copenhagen, Copenhagen; Denmark

41 (a)Dipartimento di Fisica, Università della Calabria, Rende; (b)INFN Gruppo Collegato di Cosenza, Laboratori Nazionali di Frascati; Italy

42 Physics Department, Southern Methodist University, Dallas TX; United States of America

43 Physics Department, University of Texas at Dallas, Richardson TX; United States of America

44 National Centre for Scientific Research "Demokritos", Agia Paraskevi; Greece

45 (a)Department of Physics, Stockholm University; (b)Oskar Klein Centre, Stockholm; Sweden

46 Deutsches Elektronen-Synchrotron DESY, Hamburg and Zeuthen; Germany

47 Lehrstuhl für Experimentelle Physik IV, Technische Universität Dortmund, Dortmund; Germany

48 Institut für Kern- und Teilchenphysik, Technische Universität Dresden, Dresden; Germany

49 Department of Physics, Duke University, Durham NC; United States of America

50 SUPA - School of Physics and Astronomy, University of Edinburgh, Edinburgh; United Kingdom

51 INFN e Laboratori Nazionali di Frascati, Frascati; Italy

52 Physikalisches Institut, Albert-Ludwigs-Universität Freiburg, Freiburg; Germany

53 II. Physikalisches Institut, Georg-August-Universität Göttingen, Göttingen; Germany

54 Département de Physique Nucléaire et Corpusculaire, Université de Genève, Genève; Switzerland

55 (a) Dipartimento di Fisica, Università di Genova, Genova; (b) INFN Sezione di Genova; Italy

56 II. Physikalisches Institut, Justus-Liebig-Universität Giessen, Giessen; Germany

57 SUPA - School of Physics and Astronomy, University of Glasgow, Glasgow; United Kingdom

58 LPSC, Université Grenoble Alpes, CNRS/IN2P3, Grenoble INP, Grenoble; France

59 Laboratory for Particle Physics and Cosmology, Harvard University, Cambridge MA; United States of America

60 (a) Department of Modern Physics and State Key Laboratory of Particle Detection and Electronics, University of Science and Technology of China, Hefei; (b) Institute of Frontier and Interdisciplinary Science and Key Laboratory of Particle Physics and Particle Irradiation (MOE), Shandong University, Qingdao; (c) School of Physics and Astronomy, Shanghai Jiao Tong University, Key Laboratory for Particle Astrophysics and Cosmology (MOE), SKLPPC, Shanghai; (d) Tsung-Dao Lee Institute, Shanghai; China

61 (a) Kirchhoff-Institut für Physik, Ruprecht-Karls-Universität Heidelberg, Heidelberg; (b) Physikalisches Institut, Ruprecht-Karls-Universität Heidelberg, Heidelberg; Germany

62 (a) Department of Physics, Chinese University of Hong Kong, Shatin, N.T., Hong Kong; (b) Department of Physics, University of Hong Kong, Hong Kong; (c) Department of Physics and Institute for Advanced Study, Hong Kong University of Science and Technology, Clear Water Bay, Kowloon, Hong Kong, China

63 Department of Physics, National Tsing Hua University, Hsinchu; Taiwan

64 IJCLab, Université Paris-Saclay, CNRS/IN2P3, 91405, Orsay; France

65 Department of Physics, Indiana University, Bloomington IN; United States of America

66 (a) INFN Gruppo Collegato di Udine, Sezione di Trieste, Udine; (b) ICTP, Trieste; (c) Dipartimento Politecnico di Ingegneria e Architettura, Università di Udine, Udine; Italy

67 (a) INFN Sezione di Lecce; (b) Dipartimento di Matematica e Fisica, Università del Salento, Lecce; Italy

68 (a) INFN Sezione di Milano; (b) Dipartimento di Fisica, Università di Milano, Milano; Italy

69 (a) INFN Sezione di Napoli; (b) Dipartimento di Fisica, Università di Napoli, Napoli; Italy

70 (a) INFN Sezione di Pavia; (b) Dipartimento di Fisica, Università di Pavia, Pavia; Italy

71 (a) INFN Sezione di Pisa; (b) Dipartimento di Fisica E. Fermi, Università di Pisa, Pisa; Italy

72 (a) INFN Sezione di Roma; (b) Dipartimento di Fisica, Sapienza Università di Roma, Roma; Italy

73 (a) INFN Sezione di Roma Tor Vergata; (b) Dipartimento di Fisica, Università di Roma Tor Vergata, Roma; Italy

74 (a) INFN Sezione di Roma Tre; (b) Dipartimento di Matematica e Fisica, Università Roma Tre, Roma; Italy

75 (a) INFN-TIFPA; (b) Università degli Studi di Trento, Trento; Italy

76 Institut für Astro- und Teilchenphysik, Leopold-Franzens-Universität, Innsbruck; Austria

77 University of Iowa, Iowa City IA; United States of America

78 Department of Physics and Astronomy, Iowa State University, Ames IA; United States of America

79 Joint Institute for Nuclear Research, Dubna; Russia

80 (a) Departamento de Engenharia Elétrica, Universidade Federal de Juiz de Fora (UFJF), Juiz de Fora; (b) Universidade Federal do Rio De Janeiro COPPE/EE/IF, Rio de Janeiro; (c) Instituto de Física, Universidade de São Paulo, São Paulo; Brazil

81 KEK, High Energy Accelerator Research Organization, Tsukuba; Japan

82 Graduate School of Science, Kobe University, Kobe; Japan

83 (a) AGH University of Science and Technology, Faculty of Physics and Applied Computer Science, Krakow; (b) Marian Smoluchowski Institute of Physics, Jagiellonian University, Krakow; Poland

84 Institute of Nuclear Physics Polish Academy of Sciences, Krakow; Poland

85 Faculty of Science, Kyoto University, Kyoto; Japan

86 Kyoto University of Education, Kyoto; Japan

87 Research Center for Advanced Particle Physics and Department of Physics, Kyushu University, Fukuoka; Japan

88 Instituto de Física La Plata, Universidad Nacional de La Plata and CONICET, La Plata; Argentina

89 Physics Department, Lancaster University, Lancaster; United Kingdom

90 Oliver Lodge Laboratory, University of Liverpool, Liverpool; United Kingdom

91 Department of Experimental Particle Physics, Jožef Stefan Institute and Department of Physics, University of Ljubljana, Ljubljana; Slovenia

92 School of Physics and Astronomy, Queen Mary University of London, London; United Kingdom

93 Department of Physics, Royal Holloway University of London, Egham; United Kingdom

94 Department of Physics and Astronomy, University College London, London; United Kingdom

95 Louisiana Tech University, Ruston LA; United States of America

96 Fysiska institutionen, Lunds universitet, Lund; Sweden

97 Centre de Calcul de l'Institut National de Physique Nucléaire et de Physique des Particules (IN2P3), Villeurbanne; France

98 Departamento de Física Teórica C-15 and CIAFF, Universidad Autónoma de Madrid, Madrid; Spain

99 Institut für Physik, Universität Mainz, Mainz; Germany

100 School of Physics and Astronomy, University of Manchester, Manchester; United Kingdom

101 CPPM, Aix-Marseille Université, CNRS/IN2P3, Marseille; France

102 Department of Physics, University of Massachusetts, Amherst MA; United States of America

103 Department of Physics, McGill University, Montreal QC; Canada

104 School of Physics, University of Melbourne, Victoria; Australia

105 Department of Physics, University of Michigan, Ann Arbor MI; United States of America

106 Department of Physics and Astronomy, Michigan State University, East Lansing MI; United States of America

107 B.I. Stepanov Institute of Physics, National Academy of Sciences of Belarus, Minsk; Belarus

108 Research Institute for Nuclear Problems of Byelorussian State University, Minsk; Belarus

109 Group of Particle Physics, University of Montreal, Montreal QC; Canada

110 P.N. Lebedev Physical Institute of the Russian Academy of Sciences, Moscow; Russia

111 National Research Nuclear University MEPhI, Moscow; Russia

112 D.V. Skobeltsyn Institute of Nuclear Physics, M.V. Lomonosov Moscow State University, Moscow; Russia

113 Fakultät für Physik, Ludwig-Maximilians-Universität München, München; Germany

114 Max-Planck-Institut für Physik (Werner-Heisenberg-Institut), München; Germany

115 Nagasaki Institute of Applied Science, Nagasaki; Japan

116 Graduate School of Science and Kobayashi-Maskawa Institute, Nagoya University, Nagoya; Japan

117 Department of Physics and Astronomy, University of New Mexico, Albuquerque NM; United States of America

118 Institute for Mathematics, Astrophysics and Particle Physics, Radboud UniversityNikhef, Nijmegen; Netherlands

119 Nikhef National Institute for Subatomic Physics and University of Amsterdam, Amsterdam; Netherlands

120 Department of Physics, Northern Illinois University, DeKalb IL; United States of America

121 (a) Budker Institute of Nuclear Physics and NSU, SB RAS, Novosibirsk; (b) Novosibirsk State University Novosibirsk; Russia

122 Institute for High Energy Physics of the National Research Centre Kurchatov Institute, Protvino; Russia

123 Institute for Theoretical and Experimental Physics named by A.I. Alikhanov of National Research Centre "Kurchatov Institute", Moscow; Russia

124 Department of Physics, New York University, New York NY; United States of America

125 Ochanomizu University, Otsuka, Bunkyo-ku, Tokyo; Japan

126 Ohio State University, Columbus OH; United States of America

127 Homer L. Dodge Department of Physics and Astronomy, University of Oklahoma, Norman OK; United States of America

128 Department of Physics, Oklahoma State University, Stillwater OK; United States of America

129 Palacký University, Joint Laboratory of Optics, Olomouc; Czech Republic

130 Institute for Fundamental Science, University of Oregon, Eugene, OR; United States of America

131 Graduate School of Science, Osaka University, Osaka; Japan

132 Department of Physics, University of Oslo, Oslo; Norway

133 Department of Physics, Oxford University, Oxford; United Kingdom

134 LPNHE, Sorbonne Université, Université de Paris, CNRS/IN2P3, Paris; France

135 Department of Physics, University of Pennsylvania, Philadelphia PA; United States of America

136 Konstantinov Nuclear Physics Institute of National Research Centre "Kurchatov Institute", PNPI, St. Petersburg; Russia

137 Department of Physics and Astronomy, University of Pittsburgh, Pittsburgh PA; United States of America
138 (a)Laboratório de Instrumentação e Física Experimental de Partículas - LIP, Lisboa; (b)Departamento de Física, Faculdade de Ciências, Universidade de Lisboa, Lisboa; (c)Departamento de Física, Universidade de Coimbra, Coimbra; (d)Centro de Física Nuclear da Universidade de Lisboa, Lisboa; (e)Departamento de Física, Universidade do Minho, Braga; (f)Departamento de Física Teórica y del Cosmos, Universidad de Granada, Granada (Spain); (g)Dep Física and CEFITEC of Faculdade de Ciências e Tecnologia, Universidade Nova de Lisboa, Caparica; (h)Instituto Superior Técnico, Universidade de Lisboa, Lisboa; Portugal
139 Institute of Physics of the Czech Academy of Sciences, Prague; Czech Republic
140 Czech Technical University in Prague, Prague; Czech Republic
141 Charles University, Faculty of Mathematics and Physics, Prague; Czech Republic
142 Particle Physics Department, Rutherford Appleton Laboratory, Didcot; United Kingdom
143 IRFU, CEA, Université Paris-Saclay, Gif-sur-Yvette; France
144 Santa Cruz Institute for Particle Physics, University of California Santa Cruz, Santa Cruz CA; United States of America
145 (a)Departamento de Física, Pontificia Universidad Católica de Chile, Santiago; (b)Universidad Andres Bello, Department of Physics, Santiago; (c)Instituto de Alta Investigación, Universidad de Tarapacá, Arica; (d)Departamento de Física, Universidad Técnica Federico Santa María, Valparaíso; Chile
146 Universidade Federal de São João del Rei (UFSJ), São João del Rei; Brazil
147 Department of Physics, University of Washington, Seattle WA; United States of America
148 Department of Physics and Astronomy, University of Sheffield, Sheffield; United Kingdom
149 Department of Physics, Shinshu University, Nagano; Japan
150 Department Physik, Universität Siegen, Siegen; Germany
151 Department of Physics, Simon Fraser University, Burnaby BC; Canada
152 SLAC National Accelerator Laboratory, Stanford CA; United States of America
153 Department of Physics, Royal Institute of Technology, Stockholm; Sweden
154 Departments of Physics and Astronomy, Stony Brook University, Stony Brook NY; United States of America
155 Department of Physics and Astronomy, University of Sussex, Brighton; United Kingdom
156 School of Physics, University of Sydney, Sydney; Australia
157 Institute of Physics, Academia Sinica, Taipei; Taiwan
158 (a)E. Andronikashvili Institute of Physics, Iv. Javakhishvili Tbilisi State University, Tbilisi; (b)High Energy Physics Institute, Tbilisi State University, Tbilisi; Georgia
159 Department of Physics, Technion, Israel Institute of Technology, Haifa; Israel
160 Raymond and Beverly Sackler School of Physics and Astronomy, Tel Aviv University, Tel Aviv; Israel
161 Department of Physics, Aristotle University of Thessaloniki, Thessaloniki; Greece
162 International Center for Elementary Particle Physics and Department of Physics, University of Tokyo, Tokyo; Japan
163 Department of Physics, Tokyo Institute of Technology, Tokyo; Japan
164 Tomsk State University, Tomsk; Russia
165 Department of Physics, University of Toronto, Toronto ON; Canada
166 (a)TRIUMF, Vancouver BC; (b)Department of Physics and Astronomy, York University, Toronto ON; Canada
167 Division of Physics and Tomonaga Center for the History of the Universe, Faculty of Pure and Applied Sciences, University of Tsukuba, Tsukuba; Japan
168 Department of Physics and Astronomy, Tufts University, Medford MA; United States of America
169 Department of Physics and Astronomy, University of California Irvine, Irvine CA; United States of America
170 Department of Physics and Astronomy, University of Uppsala, Uppsala; Sweden
171 Department of Physics, University of Illinois, Urbana IL; United States of America
172 Instituto de Física Corpuscular (IFIC), Centro Mixto Universidad de Valencia - CSIC, Valencia; Spain
173 Department of Physics, University of British Columbia, Vancouver BC; Canada
174 Department of Physics and Astronomy, University of Victoria, Victoria BC; Canada
175 Fakultät für Physik und Astronomie, Julius-Maximilians-Universität Würzburg, Würzburg; Germany
176 Department of Physics, University of Warwick, Coventry; United Kingdom
177 Waseda University, Tokyo; Japan

178 Department of Particle Physics and Astrophysics, Weizmann Institute of Science, Rehovot; Israel

179 Department of Physics, University of Wisconsin, Madison WI; United States of America

180 Fakultät für Mathematik und Naturwissenschaften, Fachgruppe Physik, Bergische Universität Wuppertal, Wuppertal; Germany

181 Department of Physics, Yale University, New Haven CT; United States of America

a Also at Borough of Manhattan Community College, City University of New York, New York NY; United States of America

b Also at Center for High Energy Physics, Peking University; China

c Also at Centro Studi e Ricerche Enrico Fermi; Italy

d Also at CERN, Geneva; Switzerland

e Also at CPPM, Aix-Marseille Université, CNRS/IN2P3, Marseille; France

f Also at Département de Physique Nucléaire et Corpusculaire, Université de Genève, Genève; Switzerland

g Also at Departament de Fisica de la Universitat Autonoma de Barcelona, Barcelona; Spain

h Also at Department of Financial and Management Engineering, University of the Aegean, Chios; Greece

i Also at Department of Physics and Astronomy, Michigan State University, East Lansing MI; United States of America

j Also at Department of Physics and Astronomy, University of Louisville, Louisville, KY; United States of America

k Also at Department of Physics, Ben Gurion University of the Negev, Beer Sheva; Israel

l Also at Department of Physics, California State University, East Bay; United States of America

m Also at Department of Physics, California State University, Fresno; United States of America

n Also at Department of Physics, California State University, Sacramento; United States of America

o Also at Department of Physics, King's College London, London; United Kingdom

p Also at Department of Physics, St. Petersburg State Polytechnical University, St. Petersburg; Russia

q Also at Department of Physics, University of Fribourg, Fribourg; Switzerland

r Also at Faculty of Physics, M.V. Lomonosov Moscow State University, Moscow; Russia

s Also at Faculty of Physics, Sofia University, 'St. Kliment Ohridski', Sofia; Bulgaria

t Also at Giresun University, Faculty of Engineering, Giresun; Turkey

u Also at Graduate School of Science, Osaka University, Osaka; Japan

v Also at Hellenic Open University, Patras; Greece

w Also at Institucio Catalana de Recerca i Estudis Avancats, ICREA, Barcelona; Spain

x Also at Institut für Experimentalphysik, Universität Hamburg, Hamburg; Germany

y Also at Institute for Nuclear Research and Nuclear Energy (INRNE) of the Bulgarian Academy of Sciences, Sofia; Bulgaria

z Also at Institute for Particle and Nuclear Physics, Wigner Research Centre for Physics, Budapest; Hungary

aa Also at Institute of Particle Physics (IPP); Canada

ab Also at Institute of Physics, Azerbaijan Academy of Sciences, Baku; Azerbaijan

ac Also at Instituto de Fisica Teorica, IFT-UAM/CSIC, Madrid; Spain

ad Also at Istanbul University, Dept. of Physics, Istanbul; Turkey

ae Also at Joint Institute for Nuclear Research, Dubna; Russia

af Also at Moscow Institute of Physics and Technology State University, Dolgoprudny; Russia

ag Also at National Research Nuclear University MEPhI, Moscow; Russia

ah Also at Physics Department, An-Najah National University, Nablus; Palestine

ai Also at Physikalisches Institut, Albert-Ludwigs-Universität Freiburg, Freiburg; Germany

aj Also at The City College of New York, New York NY; United States of America

ak Also at TRIUMF, Vancouver BC; Canada

al Also at Universita di Napoli Parthenope, Napoli; Italy

am Also at University of Chinese Academy of Sciences (UCAS), Beijing; China

* Deceased